a radius of 3 μm with the 408-nm laser line (100% laser power) and 17-mW optical fiber output and were imaged at interval of 1.0 s.

Minireplicon assay. 293T cells in 12-well plates were transfected with Pol I-MG (polymerase I-driven BDV minigenome [MG] construct), pc-N, pc-P, or its mutant form pc-PM1,2,3A, and pc-L as previously described (19), together with the indicated amounts of plasmid pc-XF that expresses a FLAG-tagged X protein. Forty-eight hours later, the cells were lysed, and cell lysates were prepared for chloramphenicol acetyltransferase (CAT) assays. CAT activity was quantified with a CAT enzyme-linked immunosorbent assay (Roche Molecular Diagnostics, Pleasanton, CA) according to the manufacturer's recommendations.

RESULTS

Identification of the P region required for the protein X-dependent cytoplasmic localization of P. We have documented that the intracellular localization of BDV P is influenced by its interaction with X (10), but the mechanisms underlying the X-dependent subcellular distribution of P remained unsolved. To address this question, we constructed a series of plasmids expressing X and a GFP-tagged Pwt or a GFP-tagged variety of C-terminal deletion mutants of P (Fig. 1A). Both X and P-GFP were expressed from the same bicistronic mRNA that recreated the P transcription unit responsible for X and P expression in BDV-infected cells. This approach allowed us to simultaneously examine the subcellular distribution of X and P by using an anti-X-specific serum and GFP fluorescence, respectively. Both X and P were predominantly found in the cytoplasm of cells transfected with pgX/Pwt, or pgX/PΔ1 and pgX/PΔ2, which lacked, respectively, the 31 and 36 C-terminal amino acids of P (Fig. 1B). In contrast, cells transfected with pgX/PΔ3 and pgX/PΔ4, which lacked, respectively, the 57 and 61C-terminal amino acids of P, showed a nuclear accumulation of X and P (Fig. 1B). We next examined whether the C-terminal deletion mutants of P retained their ability to interact with X. We conducted coimmunoprecipitation (CoIP) assays using lysates from OL cells cotransfected with the corresponding FLAG-tagged versions of the P constructs shown in Fig. 1A and pcXHA that expresses an HA-tagged X protein. Pwt and all the C-terminal P deletion mutants immunoprecipitated X-HA with similar efficiency (Fig. 1C). These results suggested that the formation of an X-P complex does not suffice to determine the subcellular localization of P and that the region between aa 145 to 164 of P was required for the cytoplasmic accumulation of P in the presence of X.

Role of the MetR domain of P in the cytoplasmic accumulation of the X-P complex. The region spanning aa 145 to 164 of P contains a unique methionine-rich sequence, $_{145}$**MKTM** MET-MKLMMEK$_{158}$ (methionine residues in boldface), termed the MetR, which has been suggested to stabilize the tertiary structure of P as well as participate in P interactions with other viral and cellular proteins (27, 29). To investigate the role of the MetR domain in the X-dependent subcellular distribution of P, we generated constructs pgX/PM1,2,3A, pgX/PM4,5,6A, and pgX/PM1-6A (Fig. 2A). Cells transfected with plasmids pgX/PM1,2,3A (where the first three M residues are replaced by A), pgX/PM4,5,6A, and pgX/PM1-6A exhibited a nuclear localization of P (Fig. 2B). The substitution of A for M residues might have altered the ability of P to interact with X, which could explain the nuclear, rather than cytoplasmic, accumulation of P with substitutions of A for M. To address this issue, we conducted CoIP assays using cell lysates from cells expressing an HA-tagged X and FLAG-tagged versions of Pwt or of each of the P mutants with substitutions of A for M. Our CoIP results indicated that the three P mutants with substitutions of A for M were not impaired in their ability to bind X (Fig. 2C).

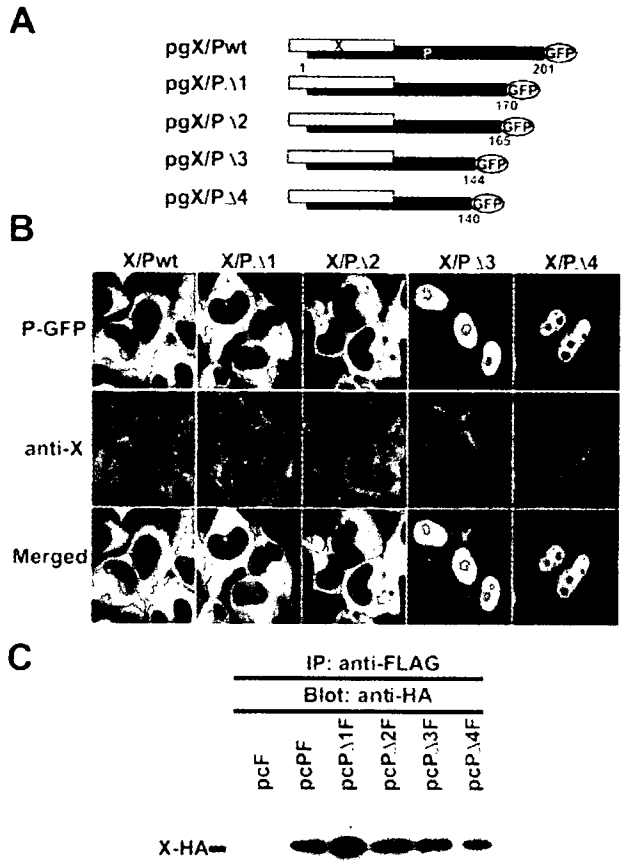

FIG. 1. Intracellular localization of deletion mutants of BDV phosphoprotein. (A) Schematic of plasmids expressing BDV X and GFP-tagged P proteins from a single mRNA that mimics the BDV bicistronic X/P mRNA. (B) Subcellular localization of BDV X and P in transfected cells. Cells were transfected with the indicated expression plasmids. P expression was monitored by GFP fluorescence, whereas X expression was examined by indirect immunofluorescence using a serum specific to X and a Cy3-labeled secondary antibody. The overlap in the distribution of X and P is revealed in the merged image. (C) CoIP of BDV P and X. OL cells were cotransfected with a plasmid expressing an HA-tagged wild-type X (Xwt) and plasmids expressing FLAG-tagged versions of the P mutant shown in panel A. Cell lysates were prepared and subjected to immunoprecipitation with an anti-FLAG antibody. Immunoprecipitated proteins were analyzed by Western blotting using an anti-HA antibody. Prior immunoprecipitation, the expression of each FLAG-tagged P and the HA-Xwt proteins was verified by Western blotting.

As with the P of other MNV, the oligomerization of BDV P is likely required for its functions (26). The P oligomerization domain has been mapped to amino acid residues 141 to 165 of P (26, 27), a region that contains the MetR domain. We therefore assessed whether the MetR mutants we generated (Fig. 2A) were competent for oligomerization. We conducted CoIP assays using cell lysates from OL cells expressing an HA-tagged Pwt and FLAG-tagged versions of either Pwt or a series

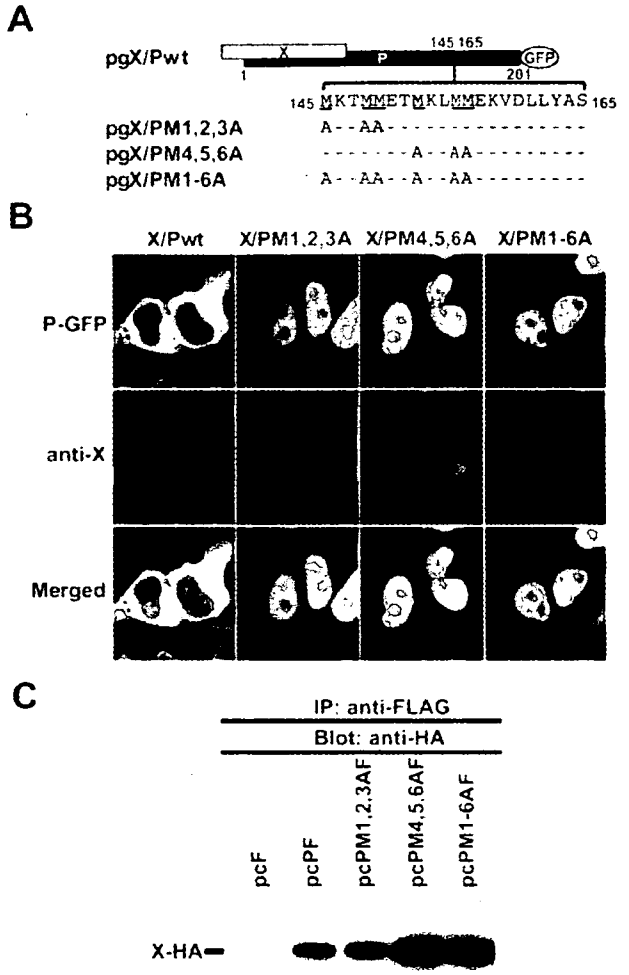

FIG. 2. Mutants with substitution in the methionine-rich region fail to localize in the cytoplasm of BDV P. (A) Schematic diagram of the MetR mutants of BDV P. Alanine (A) substitutions within the MetR domain were introduced into the plasmid pgX/Pwt. (B) Subcellular localization of BDV X and P in transfected cells. Cells were transfected with the indicated plasmids. The expression of P and X was detected by GFP-fluorescence and indirect immunofluorescence, respectively, as described in the legend of Fig. 1B. The overlap in the distribution of X and P is revealed in the merged image. (C) CoIP of BDV P and X. OL cells were cotransfected with a plasmid expressing an HA-tagged wild-type X (Xwt) and FLAG-tagged versions of P-expressing plasmids shown in panel A. Cell lysates were immunoprecipitated with an anti-FLAG antibody, and precipitants were examined by Western blotting using an anti-HA antibody. Prior to immunoprecipitation, the expression level of each recombinant protein was confirmed by Western blotting.

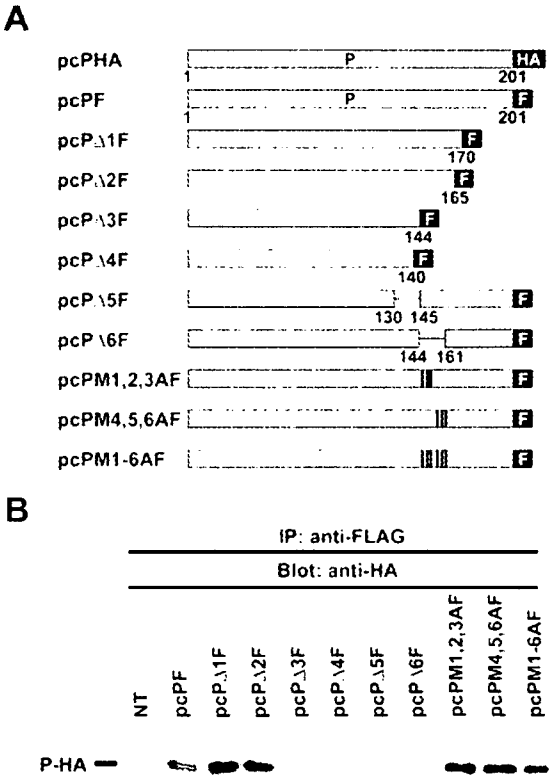

FIG. 3. Oligomerization of BDV P mutants. (A) Schematic representation of HA- and FLAG (F)-tagged Pwt and FLAG-tagged P mutants. (B) Oligomerization of BDV P mutants. OL cells were cotransfected with pcPHA expressing an HA-tagged Pwt and the indicated plasmids expressing FLAG-tagged P mutant proteins. Cell lysates were immunoprecipitated with anti-FLAG antibody, and the precipitants were detected by Western blotting with anti-HA antibody.

of P mutants (Fig. 3A). Proteins immunoprecipitated with the anti-FLAG antibody were analyzed by immunoblotting using an antibody to HA. Consistent with previous findings, P-HA was immunoprecipitated with FLAG-tagged Pwt and P mutants with C-terminal deletions of 31 (Δ1F) and 36 (Δ2F) aa, but not with P mutants lacking the 57 (Δ3F) or 61 (Δ4F) C-terminal amino acids (Fig. 3B). Notably, we found that all the P mutants within the MetR domain examined (M1,2,3AF, M4,5,6AF, and M1-6AF) could immunoprecipitate P-HA. These results indicated that the M residues within the MetR domain are not necessary for P oligomerization or for the X-P intermolecular interaction, but rather these M residues appear to play a key role in the X-dependent subcellular localization of P.

The MetR of P contains a CRM1-dependent NES. We next examined whether the MetR region of P may actively contribute to the nuclear export of P. We fused GFP to aa 145 to 165 (pGFP-PR1) and 145 to 170 (pGFP-PR2) of P (Fig. 4A). As expected, GFP alone was found in both the nucleus and cytoplasm (Fig. 4B, frame a), whereas in cells transfected with pGFP-PR plasmids, GFP expression was restricted to the cytoplasm (Fig. 4B, frames b and c), suggesting that the MetR region contains the nuclear export activity of P. To assess the contribution of the M residues within the MetR domain to the nuclear export activity of the GFP fusion peptides, we generated several mutants with substitutions of A for M residues based on plasmid pGFP-PR2 (Fig. 4A). GFP-fusion proteins were diffusely distributed in both the nucleus and cytoplasm of the cells transfected with pGFP-m1, -m2, -m3, -m5, -m6, and -m7, as well as with pGFP alone (Fig. 4B, frames d to f and h to j). In contrast, GFP expression was mainly restricted to the cytoplasm in cells transfected with pGFP-m4 (Fig. 4B, frame

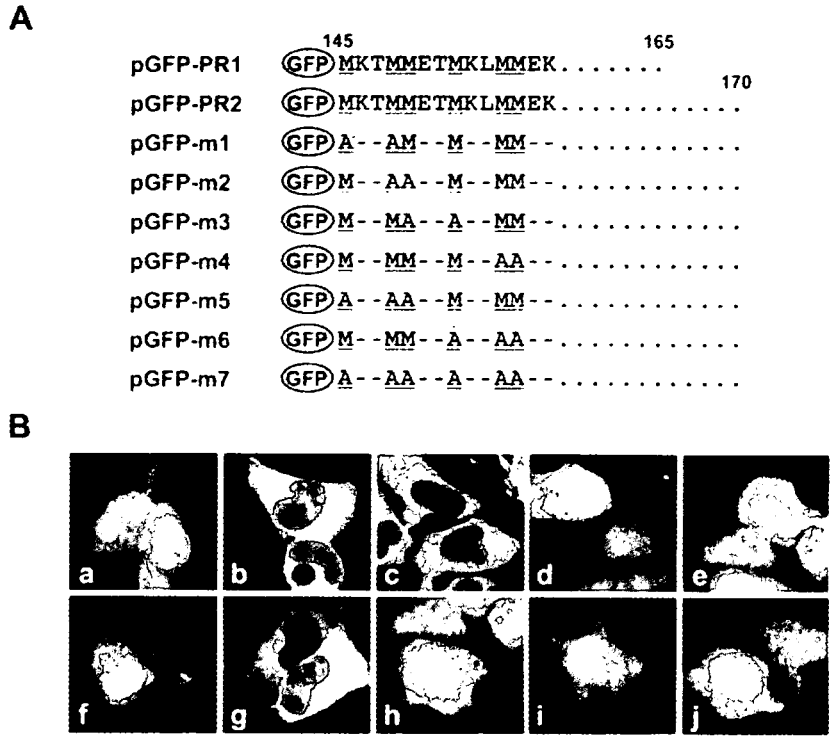

FIG. 4. BDV P nuclear export activity is mediated by its MetR domain. (A) Schematic diagram of the GFP-tagged P MetR region. Methionine (M) residues at positions 145, 148, 149, 152, 155, and 156 were replaced with alanine (A) (underlined) residues. (B) Subcellular localization of GFP fusion proteins in OL cells. Frame a, pGFP (control); frame b, pGFP-PR1; frame c, pGFP-PR2; frame d, pGFP-m1; frame e, pGFP-m2; frame f, pGFP-m3; frame g, pGFP-m4; frame h, pGFP-m5; frame i, pGFP-m6; frame j, pGFP-m7.

g). These results suggested that the MetR domain is the NES of P and that the M residues at positions 145, 148, 149, and 152 but not those at 155 and 156 are essential for the activity of this novel NES.

The nuclear export of a variety of proteins is mediated by the interaction of their respective NES and the cellular transporter receptor CRM1. The CRM1-dependent nuclear export pathway is specifically inhibited by LMB (11). Treatment with LMB of OL cells transfected with pGFP-PR1 resulted in nuclear accumulation of GFP expression (Fig. 5A), suggesting that the MetR domain mediates nuclear export of P in a CRM1-dependent manner. For further confirmation of CRM1-dependent nuclear export of BDV P, we performed RNA interference targeting CRM1 (siCRM1) as described in previous reports (13, 15). At 24 h after transfection of siCRM1 into the OL cells, the cells were further transfected with pGFP-PR1 or pgX/Pwt. Forty-eight hours posttransfection, the expression level of endogenous CRM1 was analyzed by Western blotting. As shown in Fig. 5B, this treatment specifically reduced the expression level of CRM1. The effect of the down-regulation of CRM1 on the subcellular localization of the GFP constructs containing MetR domain or full-length P was analyzed by GFP fluorescence. As shown in Fig. 5C, GFP-PR1 was found to accumulate in the nucleus of GFP expression, which was consistent with the results obtained by using LMB, whereas the down-regulation of CRM1 resulted in the predominant nuclear localization of P-GFP in the pgX/Pwt-transfected cells (Fig. 5C). This result strongly confirmed the CRM1-dependent nuclear export of BDV P.

BDV P shuttles between the nucleus and cytoplasm in the absence of X. Our finding that BDV P contains both NLS and NES suggested that P could shuttle between the nucleus and cytoplasm. To examine this possibility, we performed interspecies heterokaryon assays. Human HeLa cells transfected with a P-GFP expression plasmid (Fig. 6A, pgP) were fused to mouse NIH 3T3 cells as described above (see Materials and Methods). We monitored the nucleocytoplasmic shuttling of P by examining GFP expression in NIH 3T3 nuclei. Human and mouse cells were distinguished based on their distinct staining pattern with Hoechst 33258. As an internal control, we cotransfected HeLa cells, together with pgP, with plasmids expressing β-Gal containing the simian virus 40 T antigen NLS either alone (pCFN-βGal) or together with the human immunodeficiency virus type 1 Rev NES (pCFNrev-βGal) (Fig. 6A). P-GFP was detected in both human and mouse nuclei (Fig. 6B, frames a, b, d, and e). As predicted, β-Gal derived from pCFN-rev-βGal was also detected in both human and mouse nuclei (Fig. 6B, frames a and c), whereas β-Gal derived from pCFN-βGal lacking the Rev NES was detected only in human nuclei (Fig. 6B, frames d and f). To investigate the possible influence of X on this process, we subjected pgX/PNLS-transfected HeLa cells (Fig. 6A) to the same heterokaryon assay. GFP derived from pgX/PNLS was detected in human and mouse nuclei (Fig. 6B, frames g, h, j, and k). Likewise, as predicted,

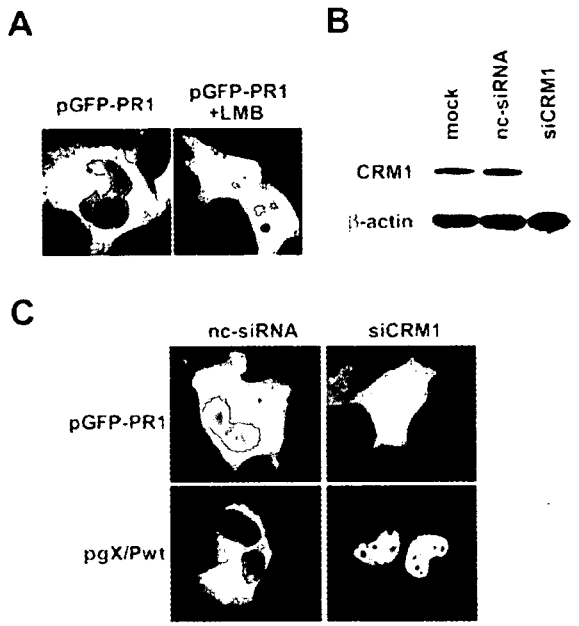

FIG. 5. The nuclear export of BDV P uses a CRM1-dependent pathway. pGFP-PR1-transfected OL cells untreated (left panel) or treated with LMB (20 ng/ml for 2 h) (right panel) were examined for GFP fluorescence after fixation. (B) OL cells were mock transfected or transfected with negative control siRNA (nc-siRNA) or siRNA for human CRM1 (siCRM1). At 48 h after the GFP construct transfection, the cells were harvested, and Western blot analysis was performed using an anti-CRM1 antibody or an anti-β-actin antibody. (C) The pGFP-PR1 or pgX/Pwt construct was transfected into the OL cells expressing negative control siRNA or siCRM1. At 48 h after transfection, GFP fusion proteins were visualized by fluorescence microscopy.

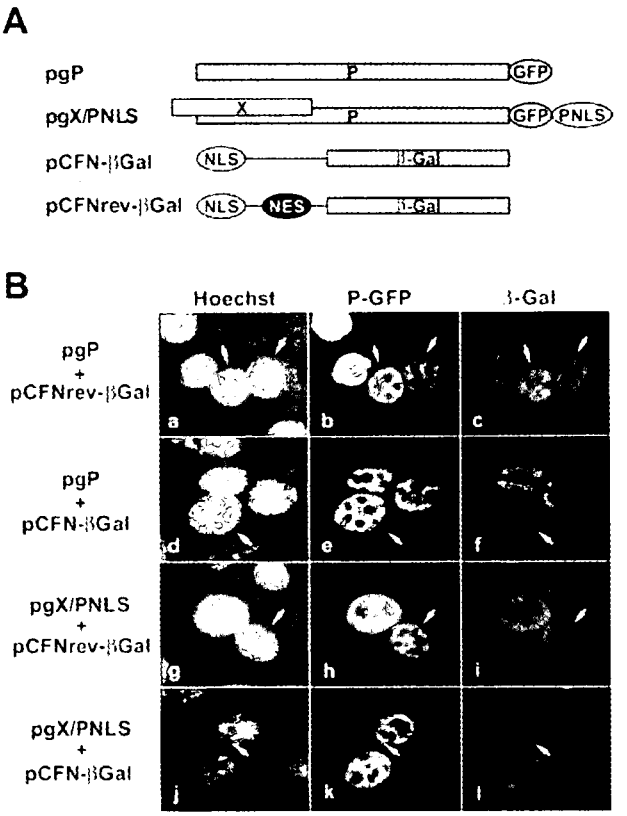

FIG. 6. BDV P shuttles between the nucleus and cytoplasm. (A) Schematic representation of the plasmids used for heterokaryon assays. (B) HeLa cells were transiently transfected with pgP and pCFNrev-βGal (frames a to c), pgP and pCFN-βGal (frames d to f), pgX/PNLS and pCFNrev-βGal (frames g to i), and pgX/PNLS and pCFN-βGal (frames j to l). Transfected cells were subjected to the interspecies heterokaryon assay as described in the text. Fields containing representative interspecies heterokaryons are shown. Frames a, d, g, and j, Hoechst staining images; frames b, e, h, and k, GFP fluorescence; frames c, f, i, and l, β-Gal staining images. Arrows indicate mouse nuclei.

β-Gal derived from pCFNrev-βGal, but not from pCFN-βGal, was also detected in both human and mouse nuclei (Fig. 6B, frames g, i, j, and l). These results indicated that P can exhibit nucleocytoplasmic shuttling activity in the absence of X.

To confirm the nucleocytoplasmic properties of BDV P, we performed a FLIP experiment using OL cells transfected with either pgPwt or pgX/PM1-6A (Fig. 2A). We subjected a defined surface (3-μm radius) of the cytoplasm of transfected cells to repeated photobleaching while monitoring the intensity of nuclear GFP fluorescence (Fig. 7). Cells transfected with pgPwt, but not with pgX/PM1-6A lacking a functional P NES, exhibited a gradual and large (>95%) decrease in nuclear GFP fluorescence over the 500-s observation period (Fig. 7). The modest decrease in GFP nuclear fluorescence observed in pgX/PM1-6A-transfected cells might be due to nuclear import of newly synthesized P. These findings further support that P is endowed with nucleocytoplasmic shuttling properties and that the M residues within the MetR domain are essential for the nuclear export of P.

Nuclear export activity of P is not critical for X-mediated inhibition of BDV MG expression. To investigate a possible role of the nuclear export of P in the virus polymerase activity, we examined the activity in the BDV minireplicon system of a P mutant, pc-PM1,2,3A, which lacked a functional NES. Although slightly lower than Pwt, mutant PM1,2,3A supported high levels of BDV RNA analogue (MG) expression (Fig. 8A), suggesting that the M residues within the MetR domain of P are not strictly required for the polymerase cofactor activity of P. BDV X is known to have a powerful inhibitory effect on BDV MG expression (19, 20). It has been suggested that X-mediated redistribution of P from the nucleus to the cytoplasm might contribute to this X inhibitory activity by affecting the assembly of the functional polymerase complex in the nucleus. We therefore investigated whether the nuclear export activity of P influences BDV polymerase activity. We compared the effect of X on BDV MG expression in cells transfected with either Pwt or the mutant PM1,2,3A lacking a functional NES. BDV MG expression was similarly inhibited in both cases (Fig. 8B), suggesting that X-mediated subcellular redistribution of P is not involved in X-mediated inhibition of the activity of the BDV polymerase.

DISCUSSION

The completion of the BDV life cycle requires a bidirectional transport of viral RNP across the nuclear envelope. In newly BDV-infected cells, the incoming viral RNP needs to be

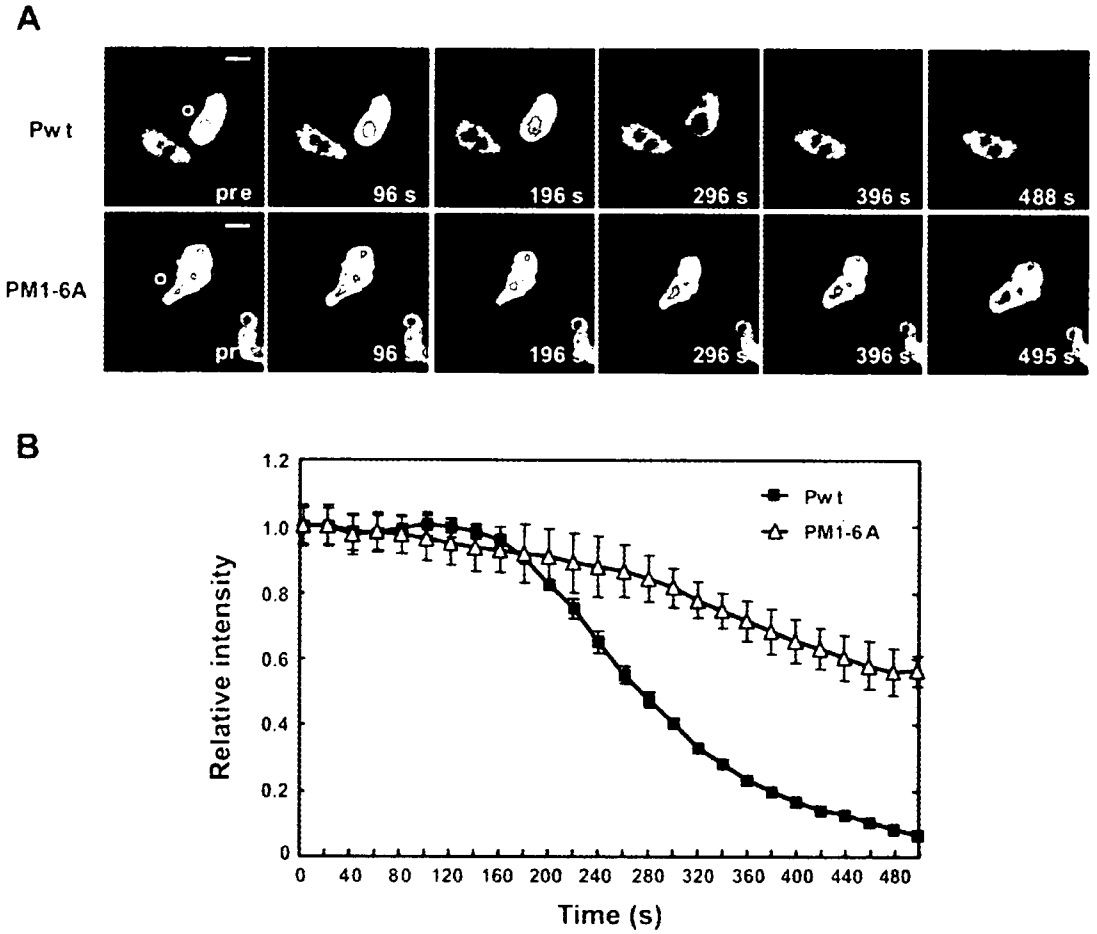

FIG. 7. BDV P dynamics in living cells. OL cells were transfected with GFP-tagged either Pwt- or PM1-6A-expressing plasmids and subjected to FLIP analysis. (A) FLIP imaging. The circled area in the cytoplasm (pre panel) was bleached repeatedly, and cells were imaged at interval of 1.0 s. A neighboring cell nucleus was not affected. Scale bars, 5 μm. (B) Quantification of GFP fluorescence in transfected OL cells. The GFP intensity was monitored in the cytoplasm in at least three different areas of transfected cells using the ImageJ program.

imported into the nucleus, where viral RNA synthesis takes place. At later stages of the infection, newly synthesized RNP must egress from the nucleus to complete the formation of infectious particles that can propagate the infection to uninfected neighboring cells. The directional control of the BDV RNP trafficking is likely determined by the ratios and interactions between viral proteins containing appropriate NLS or NES or both, as well as by host cell factors including dedicated transporters of cargo molecules carrying appropriate signals.

Bona fide NLS have been identified for BDV N (8), P (28), X (34), and L (31) proteins. These signals could contribute to the nuclear import of viral RNP, although the underlying mechanisms remain to be determined. Likewise, the signals and mechanisms by which BDV RNP egresses from the nucleus are poorly understood. We have documented that N contains a bona fide NES that utilizes a CRM1-dependent pathway for traveling through the nuclear pore complex (9). We have also shown that the intracellular distribution of BDV P is influenced by its binding to X, which promotes the cytoplasmic accumulation of P (10). Both BDV X and P contain functional NLS, suggesting that the activity of these signals must be impaired in the context of the X-P complex. The P-binding region in X completely overlaps with the NLS of X (14, 34), whereas the X-binding region in P does not involve residues contributing to any of the two NLS of P (26, 27). The apparent availability of two NLS in the X-P complex raises the question of why it is not retained in the nucleus but, rather, accumulates in the cytoplasm. An X-induced conformational change in P could impair the function of the P NLS. Alternatively, but not mutually exclusively, a functionally active NES might be present in either X or P or both, and this NES could become dominant upon formation of the X-P complex, thus leading to its efficient nuclear export. NES usually consist of four to five hydrophobic residues within a region of around 10 aa (12). The hydrophobic residues in the NES are predominantly leucine, but isoleucine, valine, methionine, and phenylalanine residues may be also tolerated (12). Several leucine- or isoleucine-rich motifs are conserved among known BDV P sequence (residues in boldface): $_{39}$**LTQPVDQLLKDL**$_{50}$, $_{73}$**LI KKLVTEL**$_{82}$ and $_{131}$**IRILGENIKIL**$_{141}$. However, our findings indicate that none of these motifs accounted for the nuclear export activity of P. Instead, we found that a hydrophobic

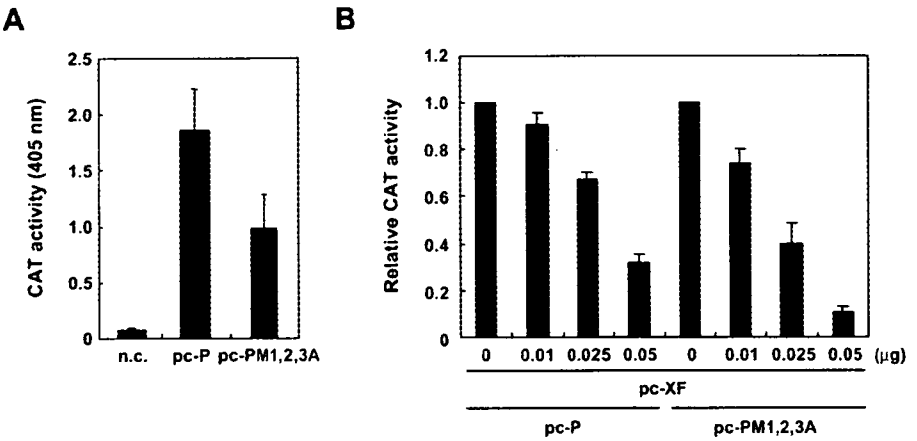

FIG. 8. The MetR mutant of P cannot escape from the inhibitory effect of X on the BDV minireplicon system. (A) NES mutant of P supports BDV polymerase activity. 293T cells were transfected with Pol I-MG (0.25 μg), pc-N (0.25 μg), pc-L (0.25 μg), and either pc-P (0.025 μg) or pc-PM1,2,3A (0.025 μg), and 48 h later CAT activity in cell lysates was determined with the CAT enzyme-linked immunosorbent assay system. n.c., negative control (mock-transfected cell lysate). (B) BDV X-mediated inhibition of BDV MG expression. 293T cells were transfected with the plasmids expressing the BDV MG RNA and supporting viral *trans*-acting factors L, N, and P, together with the indicated amounts of X expression plasmid (pc-XF). Relative CAT values from at least three independent experiments are expressed as means plus standard deviations.

region within the MetR domain spanning P residues 145 to 165 can operate as a bona fide NES to mediate CRM1-dependent nuclear export of P. The MetR domain, $_{145}$MKTMMETMKL MMEK-VDLLYAS$_{165}$, contains six M and three L residues (boldface). Substitutions of A for M dramatically affected MetR-mediated nuclear export, supporting an essential role of these M residues as part of the P NES. This finding also indicates that the L residues within domain MetR may contribute to, but are not sufficient for, this NES activity. To our knowledge, this newly identified P NES represents a unique CRM1-dependent nuclear export signal. It should be noted that a leucine-rich NES-like motif is present in the N terminus of X, but its activity as NES could not be demonstrated (14). Consistent with this, our data also indicate that this NES-like motif does not contribute to the cytoplasmic localization of the X-P complex.

Overexpression of P in infected cells drastically inhibited viral replication and transcription (6). Moreover, studies using a BDV minireplicon system have further illustrated the need of maintaining an exquisitely balanced stoichiometry of N and P for the intracellular reconstitution of a functional polymerase complex (19, 25). These results suggest that to prevent inhibition of the virus polymerase activity, BDV needs to control tightly the N/P ratio levels in the nucleus, and it is plausible that the X-dependent cytoplasmic localization of P might contribute to the regulation of the correct nuclear N/P ratio. However, we found that the BDV MG expression remained susceptible to X-mediated inhibition when the polymerase cofactor P lacked a functional NES (Fig. 8). This result indicates that X-mediated inhibition of the BDV polymerase complex is due not only to the X-dependent cytoplasmic localization of P. Because X does not appear to interfere with the binding of P to N and L (26), it seems plausible that an X-induced conformational change of P may be responsible for its polymerase inhibitory activity.

We have reported changes in the N/P ratio during the different stages of BDV infection (32, 33). Intriguingly, in BDV persistently infected cells, P was found to be present in about an eightfold molar excess over N (32). Based on data from the BDV MG rescue system, such increased P levels would be expected to result in the inhibition of the virus polymerase. A possible way for BDV to avoid this could be by also increasing levels of the X protein to help sequester the excess of P into the cytoplasm compartment or away from the site of formation of the active polymerase complex. This hypothesis would call for a regulatory mechanism, yet unknown, by which BDV could coordinate the synthesis of both P and X proteins from the same P transcriptional unit. Both BDV X and P are found in the BDV-specific nuclear speckles characteristically observed in BDV-infected cells, suggesting that the nuclear export activity of the X-P complex could be modulated by other viral or cellular proteins associated with these structures.

A detailed knowledge of the mechanisms that control the trafficking of BDV RNP would be important for a better understanding of the virus life cycle and its ability to readily establish long-term persistent infections in a variety of cell types, including postmitotic matured neurons. Studies using newly developed reverse genetic approaches will facilitate the task of elucidating the unique life cycle and pathogenesis of BDV.

ACKNOWLEDGMENTS

This article is supported by grants from the Ministry of Education, Culture, Sports, Science and Technology of Japan, a Grant-in-Aid from the Zoonosis Control Project of the Ministry of Agriculture, Forestry and Fisheries of Japan, and a Research Grant for Nervous and Mental Disorders from the Ministry of Health, Labor and Welfare of Japan.

REFERENCES

1. **Briese, T., J. C. de la Torre, A. Lewis, H. Ludwig, and W. I. Lipkin.** 1992. Borna disease virus, a negative-strand RNA virus, transcribes in the nucleus of infected cells. Proc. Natl. Acad. Sci. USA **89**:11486–11489.
2. **Cros, J. F., and P. Palese.** 2003. Trafficking of viral genomic RNA into and out of the nucleus: influenza, Thogoto and Borna disease viruses. Virus Res. **95**:3–12.

3. **Cubitt, B., C. Oldstone, and J. C. de la Torre.** 1994. Sequence and genome organization of Borna disease virus. J. Virol. **68**:1382–1396.
4. **de la Torre, J. C.** 1994. Molecular biology of Borna disease virus: prototype of a new group of animal viruses. J. Virol. **68**:7669–7675.
5. **de la Torre, J. C.** 2002. Molecular biology of Borna disease virus and persistence. Front. Biosci. **7**:D569–579.
6. **Geib, T., C. Sauder, S. Venturelli, C. Hassler, P. Staeheli, and M. Schwemmle.** 2003. Selective virus resistance conferred by expression of Borna disease virus nucleocapsid components. J. Virol. **77**:4283–4290.
7. **Goldfarb, D. S., A. H. Corbett, D. A. Mason, M. T. Harreman, and S. A. Adam.** 2004. Importin alpha: a multipurpose nuclear-transport receptor. Trends Cell. Biol. **14**:505–514.
8. **Kobayashi, T., Y. Shoya, T. Koda, I. Takashima, P. K. Lai, K. Ikuta, M. Kakinuma, and M. Kishi.** 1998. Nuclear targeting activity associated with the amino terminal region of the Borna disease virus nucleoprotein. Virology **243**:188–197.
9. **Kobayashi, T., W. Kamitani, G. Zhang, M. Watanabe, K. Tomonaga, and K. Ikuta.** 2001. Borna disease virus nucleoprotein requires both nuclear localization and export activities for viral nucleocytoplasmic shuttling. J. Virol. **75**:3404–3412.
10. **Kobayashi, T., G. Zhang, B. J. Lee, S. Baba, M. Yamashita, W. Kamitani, H. Yanai, K. Tomonaga, and K. Ikuta.** 2003. Modulation of Borna disease virus phosphoprotein nuclear localization by the viral protein X encoded in the overlapping open reading frame. J. Virol. **77**:8099–8107.
11. **Kudo, N., B. Wolff, T. Sekimoto, E. P. Schreiner, Y. Yoneda, M. Yanagida, S. Horinouchi, and M. Yoshida.** 1998. Leptomycin B inhibition of signal-mediated nuclear export by direct binding to CRM1. Exp. Cell. Res. **242**:540–547.
12. **la Cour, T., R. Gupta, K. Rapacki, K. Skriver, F. M. Poulsen, and S. Brunak.** 2003. NESbase version 1.0: a database of nuclear export signals. Nucleic Acids Res. **31**:393–396.
13. **Lund, E., S. Guttinger, A. Calado, J. E. Dahlberg, and U. Kutay.** 2004. Nuclear export of microRNA precursors. Science **303**:95–98.
14. **Malik, T. H., M. Kishi, and P. K. Lai.** 2000. Characterization of the P protein-binding domain on the 10-kilodalton protein of Borna disease virus. J. Virol. **74**:3413–3417.
15. **Miki, T., and Y. Yoneda.** 2004. Alternative splicing of Staufen2 creates the nuclear export signal for CRM1 (Exportin 1). J. Biol. Chem. **279**:47473–47479.
16. **Neumann, G., M. R. Castrucci, and Y. Kawaoka.** 1997. Nuclear import and export of influenza virus nucleoprotein. J. Virol. **71**:9690–9700.
17. **Neumann, G., M. T. Hughes, and Y. Kawaoka.** 2000. Influenza A virus NS2 protein mediates vRNP nuclear export through NES-independent interaction with hCRM1. EMBO J. **19**:6751–6758.
18. **O'Neill, R. E., J. Talon, and P. Palese.** 1998. The influenza virus NEP (NS2 protein) mediates the nuclear export of viral ribonucleoproteins. EMBO J. **17**:288–296.
19. **Perez, M., A. Sanchez, B. Cubitt, D. Rosario, and J. C. de la Torre.** 2003. A reverse genetics system for Borna disease virus. J. Gen. Virol. **84**:3099–3104.
20. **Poenisch, M., G. Unterstab, T. Wolff, P. Staeheli, and U. Schneider.** 2004. The X protein of Borna disease virus regulates viral polymerase activity through interaction with the P protein. J. Gen. Virol. **85**:1895–1898.
21. **Pollard, V. W., and M. H. Malim.** 1998. The HIV-1 Rev protein. Annu. Rev. Microbiol. **52**:491–532.
22. **Pyper, J. M., and A. E. Gartner.** 1997. Molecular basis for the differential subcellular localization of the 38- and 39-kilodalton structural proteins of Borna disease virus. J. Virol. **71**:5133–5139.
23. **Rodriguez, M. S., C. Dargemont, and F. Stutz.** 2004. Nuclear export of RNA. Biol. Cell. **96**:639–655.
24. **Sandri-Goldin, R. M.** 2004. Viral regulation of mRNA export. J. Virol. **78**:4389–4396.
25. **Schneider, U., M. Naegele, P. Staeheli, and M. Schwemmle.** 2003. Active Borna disease virus polymerase complex requires a distinct nucleoprotein-to-phosphoprotein ratio but no viral X protein. J. Virol. **77**:11781–11789.
26. **Schneider, U., K. Blechschmidt, M. Schwemmle, and P. Staeheli.** 2004. Overlap of interaction domains indicates a central role of the P protein in assembly and regulation of the Borna disease virus polymerase complex. J. Biol. Chem. **279**:55290–55296.
27. **Schwemmle, M., M. Salvatore, L. Shi, J. Richt, C. H. Lee, and W. I. Lipkin.** 1998. Interactions of the Borna disease virus P, N, and X proteins and their functional implications. J. Biol. Chem. **273**:9007–9012.
28. **Shoya, Y., T. Kobayashi, T. Koda, K. Ikuta, M. Kakinuma, and M. Kishi.** 1998. Two proline-rich nuclear localization signals in the amino- and carboxyl-terminal regions of the Borna disease virus phosphoprotein. J. Virol. **72**:9755–9762.
29. **Thierer, J., H. Riehle, O. Grebenstein, T. Binz, S. Herzog, N. Thiedemann, L. Stitz, R. Rott, F. Lottspeich, and H. Niemann.** 1992. The 24K protein of Borna disease virus. J. Gen. Virol. **73**:413–416.
30. **Tomonaga, K., T. Kobayashi, and K. Ikuta.** 2002. Molecular and cellular biology of Borna disease virus infection. Microbes Infect. **4**:491–500.
31. **Walker, M. P., and W. I. Lipkin.** 2002. Characterization of the nuclear localization signal of the Borna disease virus polymerase. J. Virol. **76**:8460–8467.
32. **Watanabe, M., Q. Zhong, T. Kobayashi, W. Kamitani, K. Tomonaga, and K. Ikuta.** 2000. Molecular ratio between Borna disease viral-p40 and -p24 proteins in infected cells determined by quantitative antigen capture ELISA. Microbiol. Immunol. **44**:765–772.
33. **Watanabe, M., B. J. Lee, W. Kamitani, T. Kobayashi, H. Taniyama, K. Tomonaga, and K. Ikuta.** 2001. Neurological diseases and viral dynamics in the brains of neonatally Borna disease virus-infected gerbils. Virology **282**: 65–76.
34. **Wolff, T., G. Unterstab, G. Heins, J. A. Richt, and M. Kann.** 2002. Characterization of an unusual importin alpha binding motif in the Borna disease virus p10 protein that directs nuclear import. J. Biol. Chem. **277**:12151–12157.

Eur Respir J 2006, 28: 51–58
DOI. 10.1183/09031936.06.00058505
Copyright©ERS Journals Ltd 2006

Carbocisteine inhibits rhinovirus infection in human tracheal epithelial cells

H. Yasuda*, M. Yamaya*, T. Sasaki*, D. Inoue*, K. Nakayama*, M. Yamada*, M. Asada*, M. Yoshida*, T. Suzuki*, H. Nishimura# and H. Sasaki*

ABSTRACT: The aim of the study was to examine the effects of a mucolytic drug, carbocisteine, on rhinovirus (RV) infection in the airways.

Human tracheal epithelial cells were infected with a major-group RV, RV14.

RV14 infection increased virus titres and the cytokine content of supernatants. Carbocisteine reduced supernatant virus titres, the amount of RV14 RNA in cells, cell susceptibility to RV infection and supernatant cytokine concentrations, including interleukin (IL)-6 and IL-8, after RV14 infection. Carbocisteine reduced the expression of mRNA encoding intercellular adhesion molecule (ICAM)-1, the receptor for the major group of RVs. It also reduced the supernatant concentration of a soluble form of ICAM-1, the number and fluorescence intensity of acidic endosomes in the cells before RV infection, and nuclear factor-κB activation by RV14. Carbocisteine also reduced the supernatant virus titres of the minor group RV, RV2, although carbocisteine did not reduce the expression of mRNA encoding a low density lipoprotein receptor, the receptor for RV2.

These results suggest that carbocisteine inhibits rhinovirus 2 infection by blocking rhinovirus RNA entry into the endosomes, and inhibits rhinovirus 14 infection by the same mechanism as well as by reducing intercellular adhesion molecule-1 levels. Carbocisteine may modulate airway inflammation by reducing the production of cytokines in rhinovirus infection.

KEYWORDS: Common cold, endosome, intercellular adhesion molecule, mucolytic drug, rhinovirus

Rhinoviruses (RVs) are the major cause of the common cold and the most common acute infectious illnesses in humans [1]. RVs are also associated with acute exacerbations of bronchial asthma [2] and chronic obstructive pulmonary disease (COPD) [3]. Several mechanisms of action have been proposed, and the manifestations of RV-induced pathogenesis are thought to be the result of virus-induced mediators of inflammation [3–5].

RV infection induces the production of cytokines, including interleukin (IL)-1, IL-6 and IL-8 [5–7]. These cytokines exert pro-inflammatory effects [8] and may be related to the pathogenesis of RV infections. Mucolytic or mucoactive drugs, such as L-carbocisteine or carbocysteine lysine salt monohydrate (SCMC-Lys), are used clinically in patients with COPD and bronchial asthma in various countries, including Japan and Italy [9]. SCMC-Lys reduces the concentration of IL-6 in the breath condensate of acute COPD patients [10], suggesting anti-inflammatory effects of SCMC-Lys in COPD. SCMC-Lys [11] and *S*-carboxymethylcysteine (SCMC) [12] also reduce the number of inflammatory cells in airways after exposure to cigarette smoke or sulphur dioxide in rats, and inhibit neutrophil activation [13]. These findings are suggestive of anti-inflammatory effects of mucolytic drugs, including carbocysteine. However, the effects of carbocisteine on cytokine production in airway epithelial cells with RV infections have not been studied.

Recent reports have revealed that the major group of RVs enter the cytoplasm of infected cells after binding to their receptor intercellular adhesion molecule (ICAM)-1 [14, 15]. The entry of the RNA of a major group RV, RV14, into the cytoplasm of infected cells is thought to be mediated by destabilisation from receptor binding and endosomal acidification [15]. Macrolide antibiotics, such as bafilomycin [16, 17] and erythromycin [7], inhibit infection by the major group of RVs *via* a reduction in ICAM-1 expression [7, 17] and an increase in endosomal pH [7, 16]. Glucocorticoid also inhibits RV14 infection *via* reduction of ICAM-1 expression [18]. Airway inflammation induced by viral infections, including RV infections, is associated with

AFFILIATIONS
*Dept of Geriatric and Respiratory Medicine, Tohoku University School of Medicine, and
#Virus Research Centre, Clinical Research Division, Sendai National Hospital, Sendai, Japan.

CORRESPONDENCE
H. Yasuda
Dept of Geriatric and Respiratory Medicine
Tohoku University School of Medicine
1-Seiryo-machi
Aoba-ku
Sendai 980-8574
Japan
Fax. 81 227177186
E-mail. yasuda@geriat.med.tohoku.ac.jp

Received:
May 18 2005
Accepted after revision.
February 17 2006

SUPPORT STATEMENT
This study was supported by Grants-In-Aid for Scientific Research from the Ministry of Education, Science and Culture of the Japanese government (Tokyo, Japan) to M. Yamaya (16590732) and H. Yasuda (17790524), a grant from Japanese Foundation for Aging and Health (Aichi, Japan) to K. Nakayama, and Health and Labour Sciences Research Grants for Research on Measures for Intractable Diseases from the Ministry of Health, Labour and Welfare of the Japanese government (Tokyo, Japan) to M. Yamaya (17243601).

European Respiratory Journal
Print ISSN 0903-1936
Online ISSN 1399-3003

exacerbations of COPD [3, 4]. SCMC-Lys prevents acute exacerbations of COPD [9]. However, the mechanisms, other than anti-inflammatory effects in COPD [10], are still uncertain. Conversely, *N*-acetylcysteine, another mucolytic drug, reduces the expression of ICAM-1 in the lung [19]. Therefore, it is conceivable that carbocisteine may modulate the function of airway epithelial cells, including expression of ICAM-1, and may inhibit RV infection. However, the effects of carbocisteine on RV infection have not been studied.

Therefore, the effects of carbocisteine on RV infection in human airway epithelial cells were studied. The effects of carbocisteine on the production of ICAM-1 and cytokines, and on endosomal pH, were also examined in order to clarify the mechanisms responsible for the inhibition of RV infection.

MATERIALS AND METHODS

Patient characteristics

Tracheae for cell culture were obtained after death from 25 patients (mean age 64±2 yrs; 10 female, 15 male) under a protocol approved by the Ethics Committee of Tokohu University School of Medicine. The causes of death included acute myocardial infarction (n=8), malignant tumour other than lung cancer (n=8), cerebral bleeding (n=3), rupture of an aortic aneurysm (n=2), renal failure (n=2), congestive heart failure (n=1) and malignant lymphoma (n=1).

Human tracheal epithelial cell culture

Isolation and culture of the human tracheal surface epithelial cells were performed as described previously [7, 17].

Viral stocks and detection and titration of viruses

Stocks of a minor group RV, RV2, and a major group RV, RV14, were prepared from patients with common colds by infecting human embryonic fibroblast cells as described previously [7, 17]. Detection and titration of RVs were performed by observing the cytopathic effects of the viruses on the fibroblast cells using previously described methods [7, 17], and the amount of specimen required to infect 50% of the fibroblast cells (50% tissue culture infective dose ($TCID_{50}$)) was determined.

Detection and quantification of rhinovirus RNA

Detection and quantification of RV14 RNA in human tracheal epithelial cells were performed by RT-PCR as previously described [7, 17]. In addition, in order to quantify RV14 RNA and reduced glyceraldehye-3-phosphate dehydrogenase mRNA expression in the cells after RV infection, real-time quantitative RT-PCR, using the Taqman technique (Roche Molecular Diagnostic Systems, Foster, CA, USA), was performed as previously described [17, 20–22]. The program PrimerExpress (Applied Biosystems, Foster, CA, USA) was used to design the probe and primers based on guidelines for the optimal performance of the PCR [7, 17].

Measurement of lactate dehydrogenase concentration

The amount of lactate dehydrogenase (LDH) in the culture supernatants was measured using the method described by AMADOR *et al.* [23].

Effects of carbocisteine on viral infection

In order to examine the effects of carbocisteine on viral titres and the cytokine content of supernatants, and the mRNA expression of ICAM-1, the receptor for the major group of RVs [14], and the low-density lipoprotein (LDL) receptor, the receptor for the minor group of RVs [24], and RV14 RNA expression, the cells were treated with 10 μM carbocisteine or vehicle (PBS) beginning 3 days before RV infection and continuing until the end of the experiments [17]. This timeframe was chosen because the maximum concentrations of SCMC in the serum become >10 μM after oral ingestion of 1,500 mg SCMC [25]. The cells were then exposed to RV2 (1×10^5 $TCID_{50}\cdot mL^{-1}$), RV14 (1×10^5 $TCID_{50}\cdot mL^{-1}$) or vehicle (Eagle's minimum essential medium) for 60 min and cultured at 33°C with rolling, as described previously [7, 17].

Study protocol

In order to measure the time course of viral release during the first 24 h, four separate cultures from the same trachea were used, and the results calculated from seven different tracheae. The culture supernatants were collected at either 1, 6, 12 or 24 h after RV14 infection. In order to measure viral titre during the 24–48 h after RV infection, supernatants were also collected at 48 h after RV infection. The viral content of the supernatant was expressed in $TCID_{50}$ units per millilitre.

In order to examine the concentration-dependent effects of carbocisteine on RV infection, cells were treated with carbocisteine at concentrations ranging 0.01–30 μM.

The effects of carbocisteine on susceptibility to RV14 infection were evaluated as previously described [6, 7], using epithelial cells pre-treated with carbocisteine (10 μM, 3 days) or vehicle (PBS, 3 days). The cells were then exposed to serial 10-fold dilutions of RV14 or vehicle (Eagle's minimum essential medium) for 1 h at 33°C. The presence of RV14 in the supernatants collected 1–3 days after infection was determined using the human embryonic fibroblast cell assay, described above, in order to assess whether infection occurred at each RV dose used.

Measurement of intercellular adhesion molecule-1 and low-density lipoprotein receptor expression

The mRNAs of ICAM-1 and LDL receptor were examined using real-time RT-PCR analysis as previously described [7]. In addition, concentrations of a soluble form of ICAM-1 (sICAM-1) were measured in culture supernatants using an enzyme immunoassay.

Effects of carbocisteine on cytokine production

IL-1β, IL-6, IL-8 and tumour necrosis factor (TNF)-α were measured in culture supernatants using specific ELISAs [7].

Measurement of changes in acidic endosome distribution

The fluorescence intensity of acidic endosomes in the cells was measured, as previously described, using a dye, LysoSensor DND-189 (Molecular Probes, Eugene, OR, USA) [7, 17], from 100 s before to 300 s after the treatment with carbocisteine (10 μM) or vehicle (PBS).

Isolation of nuclear extracts and electrophoretic mobility shift assays

The extraction of nuclei and electrophoretic mobility shift assays were performed as previously described [7].

Statistical analysis

Results are expressed as mean±SEM. Statistical analysis was performed using two-way repeated ANOVA. Subsequent *post hoc* analysis was performed using Bonferroni's method. For all analyses, values of $p<0.05$ were assumed to be significant (n=number of donors (tracheae) whose cultured epithelial cells were used).

RESULTS

Effects of carbocisteine on rhinovirus infection in human tracheal epithelial cells

Exposing confluent human tracheal epithelial cell monolayers to RV2 (1×10^5 $TCID_{50}\cdot mL^{-1}$) and RV14 (1×10^5 $TCID_{50}\cdot mL^{-1}$) consistently led to infection. No detectable virus was revealed 1 h after infection. RV2 and RV14 were detected in culture medium at 6 h, and the viral content progressively increased during the period 6–24 h after infection (fig. 1a and c). Viral titres of supernatants collected 1–2 days after infection also contained significant levels of RV2 and RV14 (fig. 1a and c). Supernatant viral titres increased significantly with time for the first 48 h ($p<0.05$ using ANOVA).

Treatment of the cells with carbocisteine significantly decreased the titres of RV2 and RV14 in supernatants 24 and 48 h after infection (fig. 1a and c). Furthermore, carbocisteine inhibited RV2 and RV14 infection in a concentration-dependent manner, the maximum effect being obtained at 10 and 30 μM (fig. 1b and d).

In order to determine whether or not RV14 infection or carbocisteine-induced cytotoxic effects on the cultured cells caused cell detachment from the tubes after the cells had formed a confluent sheet, cell numbers were counted after RV14 infection and after treatment with carbocisteine. Cell numbers were constant in the confluent epithelial cells in the control medium, and the coefficient of variation was small (7.3%; n=15). Neither RV14 infection (1×10^5 $TCID_{50}\cdot mL^{-1}$; 2 days) nor carbocisteine treatment (10 μM; 5 days) had any effect on cell number (data not shown). Cell viability, assessed by trypan blue exclusion [7], was consistently >96% in the carbocisteine-treated culture. RV14 infection and carbocisteine treatment (10 μM) did not alter the amount of LDH in the supernatants. The amount of LDH in the supernatants was 29±2 $IU\cdot L^{-1}$ before RV14 infection, 30±2 $IU\cdot L^{-1}$ 2 days after RV14 infection ($p>0.50$; n=5), and 30±2 $IU\cdot L^{-1}$ after carbocisteine treatment (10 μM; 5 days) ($p>0.50$; n=5).

Effects of carbocisteine on viral RNA by PCR

No detectable RV14 was revealed before RV14 infection (data not shown). RV14 was detected 24 h after RV14 infection

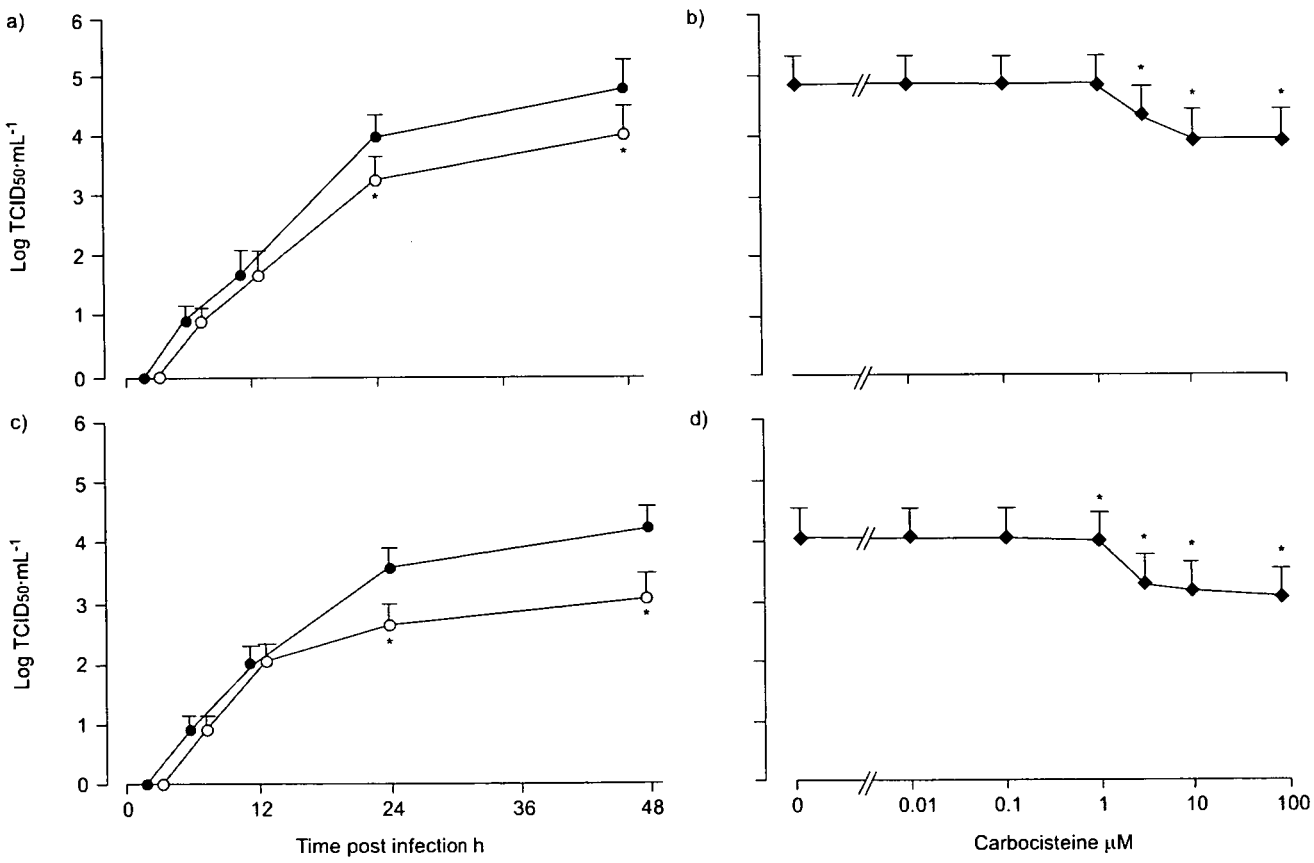

FIGURE 1. Viral titres (50% tissue culture infective dose ($TCID_{50}$) per millilitre) in supernatants of human tracheal epithelial cells obtained: a, c) at different times after exposure to 1×10^5 $TCID_{50}\cdot mL^{-1}$ rhinovirus (RV)14 (a) and RV2 (c) in the presence (○) of carbocisteine (10 μM) or vehicle (PBS; ●); and b, d) at different concentrations of carbocisteine 24–48 h after infection with RV14 (b) and RV2 (d). The cells were treated with carbocisteine or vehicle beginning 3 days before RV14 infection and continuing the end of the experiments. Data are presented as mean±SEM (n=5 tracheae). *: $p<0.05$ *versus* vehicle.

(fig. 2a), and the amount of RV14 RNA in the cells was greater at 48 h than at 24 h (fig. 2b). Carbocisteine (10 μM) caused a decrease in the amount of RV14 RNA in the cells 24 and 48 h after infection (fig. 2b). The magnitude of the inhibitory effects of carbocisteine 48 h after infection was greater than that at 24 h (fig. 2b).

Effects of carbocisteine on susceptibility to rhinovirus 14 infection

Treatment of the cells with carbocisteine decreased their susceptibility to infection by RV14. The minimum dose of RV14 necessary to cause infection in cells treated with carbocisteine (10 μM; 3 days) (2.6 ± 0.2 log $TCID_{50} \cdot mL^{-1}$; $p<0.05$; $n=5$) was significantly higher than that in cells treated with vehicle (PBS) (1.8 ± 0.2 log $TCID_{50} \cdot mL^{-1}$; $n=5$).

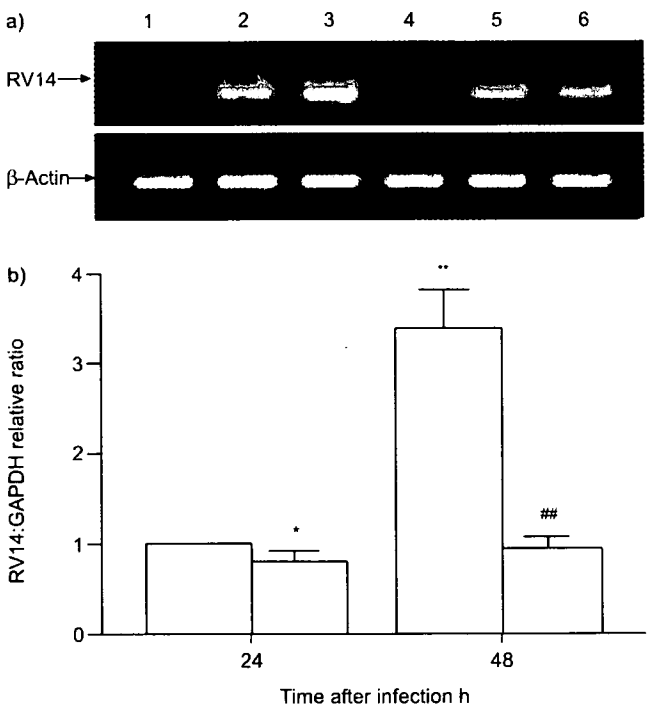

FIGURE 2. a) Replication of rhinovirus (RV) 14 RNA (381 bp) from human tracheal epithelial cells 0, 24 and 48 h (lanes 1–3 and 4–6, respectively) after RV14 infection in the presence of 10 μM carbocisteine (lanes 4–6) or vehicle (PBS) alone (lanes 1–3) as detected by RT-PCR (β-actin RNA 217 bp). Data are representative of three different experiments. b) Corresponding data obtained by real-time quantitative RT-PCR (□: carbocisteine; ▨: vehicle). A standard curve was constructed using the fluorescence emission signals and the cycle threshold by means of 10-fold dilutions of the total RNA, extracted from 1×10^5 of the 50% tissue culture infective dose ($TCID_{50} \cdot mL^{-1}$ RV14 in the supernatants of human embryonic fibroblasts 7 days after RV14 infection (1×10^4 $TCID_{50} \cdot mL^{-1}$). Real-time quantitative RT-PCR for reduced glyceraldehye-3-phosphate dehydrogenase (GAPDH) was also performed using the same PCR products. RV RNA expression was normalised to the constitutive expression of GAPDH mRNA and expressed relative to cells treated with vehicle alone 24 h after infection. Data are presented as mean±SEM ($n=5$ tracheae). *: $p<0.05$; **: $p<0.01$ *versus* vehicle 24 h after infection; ##: $p<0.01$ *versus* vehicle 48 h after infection.

Effects of carbocisteine on expression of intercellular adhesion molecule-1

Carbocisteine inhibited baseline ICAM-1 mRNA expression in the cells before RV14 infection (fig. 3a). Carbocisteine reduced ICAM-1 mRNA expression by >50% compared with that of cells treated with vehicle (PBS) (fig. 3a). Likewise, carbocisteine significantly reduced supernatant sICAM-1 concentrations before RV14 infection (fig. 3b). In contrast, carbocisteine did not inhibit baseline LDL receptor mRNA expression in the cells before RV14 infection (fig. 3c).

Effects of carbocisteine on cytokine production

Carbocisteine reduced the baseline secretion of IL-6 and IL-8 for 24 h before RV14 infection compared with that in the cells treated with vehicle (PBS) (table 1). Furthermore, the secretion of IL-6 and IL-8 increased 24 h after RV14 infection. Carbocisteine also reduced the RV14 infection-induced secretion of IL-6 and IL-8 compared to that in the cells treated with vehicle 24 h after RV14 infection (table 1).

Conversely, carbocisteine inhibited the baseline secretion of IL-1β for 24 h before RV14 infection compared with that in cells with no carbocisteine treatment (table 1). In contrast, the secretion of IL-1β 24 h after RV14 infection did not differ from that before RV14 infection (table 1). TNF-α was not detectable in supernatants for 24 h before and after RV14 infection.

Effects of carbocisteine on the acidification of endosomes

Acidic endosomes in human tracheal epithelial cells were stained green using LysoSensor DND-189. Green fluorescence from acidic endosomes was observed in a granular pattern in the cytoplasm (data not shown), as previously described [7]. Carbocisteine decreased the number and fluorescence intensity

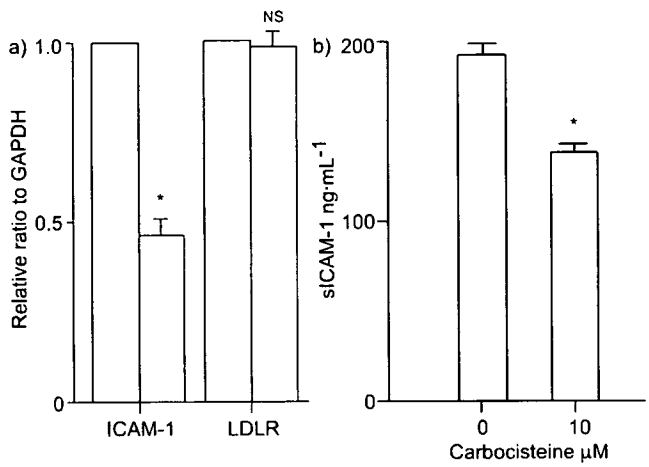

FIGURE 3. a) Expression of intercellular adhesion molecule (ICAM)-1 and low-density lipoprotein receptor (LDLR) mRNA in human tracheal epithelial cells 3 days after starting treatment with 10 μM carbocisteine (□) or PBS vehicle (▨) detected by real-time quantitative RT-PCR. mRNA expression was normalised to the constitutive expression of reduced glyceraldehyde-3-phosphate dehydrogenase (GAPDH) mRNA. b) Soluble ICAM (sICAM)-1 concentration in cell supernatants 3 days after starting treatment with 10 μM carbocisteine or vehicle (0 μM carbocisteine). The medium was changed daily, and the supernatants collected 2–3 days after starting treatment. Results are mean±SEM ($n=5$ tracheae). NS: nonsignificant (*versus* control); *: $p<0.05$ *versus* control.

TABLE 1 Effects of carbocisteine on supernatant cytokine contents before and 24 h after rhinovirus (RV) 14 infection

	Before infection		After infection	
	Control	Treated	Control	Treated
IL-1β pg·mL^{-1}	71±5	40±3*	72±5	39±3*
IL-6 pg·mL^{-1}	64±4	36±3*	219±23*	123±15*,#
IL-8 pg·mL^{-1}	542±41	517±37*	826±44*	491±58*,#

Data are presented as mean±SEM (n=5 for all). Human tracheal cells were treated with either carbocisteine or PBS vehicle (control). *: $p<0.05$ *versus* control before infection. #: $p<0.05$ *versus* control 24 h after infection. IL: interleukin.

of acidic endosomes with green fluorescence in the cells over time (fig. 4a). The fluorescence intensity of acidic endosomes in the epithelial cells treated with carbocisteine for 300 s was significantly reduced (fig. 4).

Nuclear factor-κB DNA-binding activity in human tracheal epithelial cells

Baseline nuclear factor (NF)-κB DNA-binding activity was constant, and increased activation of NF-κB DNA-binding activity was present in the cells 120 min after RV14 infection (fig. 5), as previously described [7]. Carbocisteine reduced the increased activation of NF-κB occurring as a result of RV14 infection (fig. 5).

DISCUSSION

In the present study, it has been shown that a mucolytic drug, carbocisteine, reduced supernatant viral titres and viral RNA levels of a major group RV, RV14, in cultured human tracheal epithelial cells. Pretreatment with carbocisteine inhibited the expression of mRNA encoding ICAM-1, the receptor for the major group of RVs [14], as well as the supernatant concentrations of sICAM-1 before RV14 infection. Since the minimum dose of RV14 necessary to cause infection in cells treated with carbocisteine was significantly higher than that in cells treated with vehicle, carbocisteine may inhibit RV14 infection, at least partly, by reducing the production of its receptor, ICAM-1, as observed in human tracheal epithelial cells treated with dexamethasone [18] and erythromycin [7]. Furthermore, carbocisteine reduced the fluorescence intensity of acidic endosomes in the epithelial cells. The magnitude of the inhibitory effects of carbocisteine on the fluorescence intensity of acidic endosomes was similar to that of bafilomycin A_1 [17] and erythromycin [7]. Conversely, carbocisteine also reduced supernatant virus titres of a minor group RV, RV2, although it did not reduce the mRNA expression of the LDL receptor, the receptor for the minor group of RVs [24]. Carbocisteine may also inhibit RV2 and RV14 RNA entry across acidic endosomes, as demonstrated in HeLa cells and human tracheal epithelial cells treated with bafilomycin A_1 [16, 17, 26] and erythromycin [18].

Various viruses have been reported to be responsible for exacerbations of disease in patients with COPD and bronchial

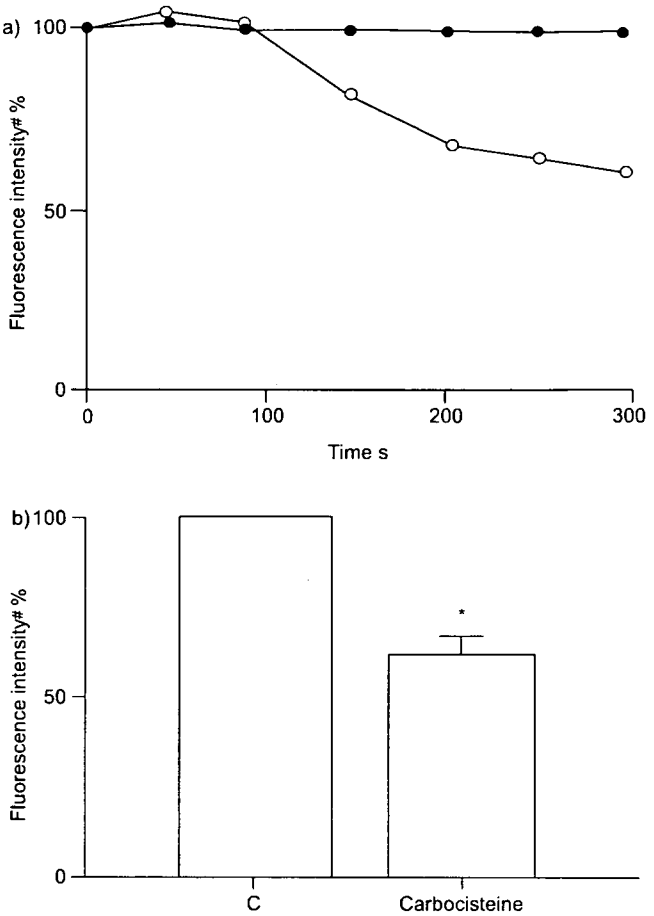

FIGURE 4. a) Time course of changes in the intensity of green fluorescence from acidic endosomes in human tracheal epithelial cells after treatment with either 10 μM carbocisteine (○) or PBS vehicle (●). Inhibitors were administrated at time 0. b) Fluorescence intensity of acidic endosomes 300 s after the addition of 10 μM carbocisteine or vehicle (control (C)). The fluorescence intensity of acidic endosomes was measured in 100 human tracheal epithelial cells, and the mean expressed as a percentage of the control value (#). Data are presented as mean±SEM (n=5 tracheae). *: $p<0.05$ *versus* control.

asthma, including RVs, influenza virus and respiratory syncytial virus [2–4]. SEEMUNGAL *et al.* [3] reported that 64% of COPD exacerbations were associated with a cold before the onset of exacerbations; 77 viruses were detected in 39% of COPD exacerbations, and 39 (58%) of these viruses were RVs. RVs are also associated with acute exacerbations in bronchial asthma [2]. These findings suggest that RVs may be a major pathogen responsible for acute exacerbations of COPD and bronchial asthma.

Various mechanisms have been attributed to the pathogenesis of COPD and bronchial asthma exacerbations, including airway inflammation, airway oedema, bronchoconstriction and mucus hypersecretion [4]. In addition, neutrophilic and eosinophilc inflammation in the exacerbations are associated with a variety of mediators, including IL-6 and IL-8, and the production and secretion of IL-6 and IL-8 are stimulated by RV14 in airway epithelial cells, as shown in the present study as well as previous studies [5–7]. Furthermore, ICAM-1

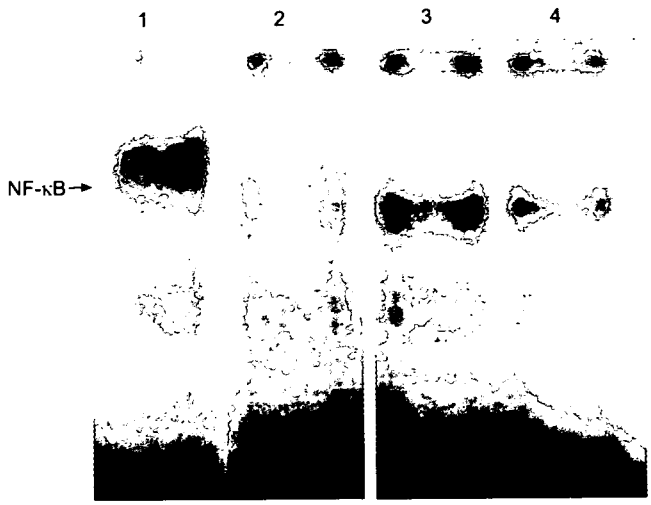

FIGURE 5. Nuclear factor (NF)-κB DNA-binding activity of human tracheal epithelial cells before (lane 2) and 120 min after (lanes 3 and 4) rhinovirus (RV) 14 infection in the presence of 10 μM carbocisteine (lane 4) or PBS vehicle (lane 3) detected *via* electrophoretic mobility shift assay (lane 1: positive control (10 ng·mL^{-1} IL-1β plus 10 ng·mL^{-1} tumour necrosis factor-α for 24 h)). The cells were treated with carbocisteine or vehicle from 3 days before until 120 min after RV14 infection. Data are representative of three different experiments.

interacts physiologically with leukocyte function-associated antigen-1, expressed on leukocytes, and thus plays a vital role in the recruitment and migration of immune effector cells to sites of local inflammation, as observed in patients with COPD [27]. Therefore, reduced RV14 infection-induced production of IL-6 and IL-8 by carbocisteine, observed in the present study, may be associated with the modulation of airway inflammation after RV infection, and with the prevention of acute exacerbations of chronic obstructive bronchitis, as previously described [9].

In the present study, carbocisteine reduced the baseline production of cytokines, including IL-1β, IL-6 and IL-8, as well as ICAM-1, before RV14 infection. RV14 infection increased the production of IL-6 and IL-8, and carbocisteine also reduced RV14 infection-induced production of IL-6 and IL-8. The concentration of IL-1β in supernatants had not changed 24 h after RV14 infection, and TNF-α was not detectable in supernatants 24 h after RV14 infection, as previously reported [7, 18]. Since carbocisteine reduced the RV14 titre in supernatants, the inhibitory effects of carbocisteine on RV14 infection, and on cytokine production itself, might be associated with the reduced production of IL-6 and IL-8 in the cells treated with carbocisteine after RV14 infection.

Increased activation of NF-κB was also apparent in cells 120 min after RV14 infection, as shown in previous studies [5, 7], and carbocisteine inhibited this activation. NF-κB increases the expression of genes encoding many cytokines, such as IL-6, IL-8 and ICAM-1 [5]. Therefore, a reduction in cytokine and ICAM-1 levels might be mediated *via* the carbocisteine-reduced activation of NF-κB.

Endosomal pH is thought to be regulated by vacuolar H^+-ATPases [28] and ion transport across Na^+/H^+ antiporters [28]. The inhibitors of Na^+/H^+ antiporters, 5-(*N*-ethyl-*N*-isopropyl)amiloride and *N''*-[5-hydroxymethyl-3-(1H-pyrrol-1-yl)benzoyl]guanidine methanesulphonate (FR168888), as well as a vacuolar H^+-ATPase inhibitor, bafilomycin, increase endosomal pH and inhibit RV14 infection in cultured human tracheal epithelial cells [7]. Although there are no data to support this, the increased endosomal pH induced by carbocisteine in the present study may be associated with an inhibitory effect on vacuolar H^+-ATPases or Na^+/H^+ antiporters in airway epithelial cells.

Recent reports revealed that the major group of RVs enters the cytoplasm of infected cells after binding to its receptor, ICAM-1 [14]. The entry of the RNA of a major group RV, RV14, into the cytoplasm of infected cells is thought to be mediated by destabilisation from receptor binding and endosomal acidification [15]. The inhibitory effects of carbocisteine on infection by RV14 and its effects on endosomal pH in the present study are consistent with those of bafilomycin and erythromycin in previous studies [7, 16, 17]. In addition, the inhibitory effects of carbocisteine on ICAM-1 expression in airway epithelial cells might also be associated with inhibitory effects on RV14 infection, as previously reported for the inhibitory effects of bafilomycin, erythromycin and dexamethasone [7, 17, 18].

In the present study, the inhibitory effects of carbocisteine were observed over a small range of concentrations, and there is no complete inhibition of infection. The precise reason for this is uncertain. However, the magnitude of the inhibitory effects of carbocisteine on supernatant RV titres was smaller than those of dexamethasone and erythromycin [7, 18]. The weak inhibitory effects of carbocisteine might show a small range of response and incomplete inhibition of infection. The magnitude of the inhibitory effects of carbocisteine on supernatant sICAM-1 concentrations was smaller than those of dexamethasone and erythromycin on ICAM-1 protein expression [7, 18], although the magnitude of the inhibitory effects of carbocisteine on the fluorescence intensity of acidic endosomes was similar to those of bafilomycin A_1 [17] and erythromycin [7]. Therefore, smaller inhibitory effects of carbocisteine on ICAM-1 expression might be partly associated with lesser inhibition by carbocisteine of RV infection compared with the inhibitory effects of dexamethasone and erythromycin.

Carbocysteine exerts an anti-oxidant action by scavenging reactive oxygen intermediates [29]. Indeed, SCMC-Lys reduces the concentration of 8-isoprostane, a prostaglandin-like compound, during peroxidation of membrane phospholipids by reactive oxygen species in the breath condensate of acute COPD patients [10]. Furthermore, bafilomycin A_1, a blocker of vacuolar H^+-ATPase, reduces endosome acidification [17] in airway epithelial cells and reduces production of reactive oxygen species in alveolar macrophages [30], suggesting a relationship between antioxidant effects and the reduced acidification of endosomes. Reduced production of inflammatory cytokines and ICAM-1 by carbocisteine, in the present study, also suggests anti-inflammatory effects of carbocisteine, as shown in previous studies that demonstrated reduced IL-6 concentrations in breath condensate caused by SCMC-Lys in COPD patients [10] and reduced numbers of inflammatory cells in airways in rats caused by SCMC-Lys [11] and SCMC [12].

In summary, this is the first report that a mucolytic drug, carbocisteine, inhibits infection by rhinovirus 14 and decreases the susceptibility of cultured human tracheal epithelial cells to rhinovirus 14 infection, probably through the inhibition of intercellular adhesion molecule-1 expression and endosomal acidification. Carbocisteine also inhibited rhinovirus 2 infection, probably through the inhibition of endosomal acidification. Carbocisteine reduced baseline and rhinovirus infection-induced release of pro-inflammatory cytokines, such as interleukin-6 and -8, in supernatants. Carbocisteine may inhibit infection by the major and minor group of rhinoviruses, and modulate inflammatory responses in the airway epithelial cells after rhinovirus infection.

ACKNOWLEDGEMENTS

The authors would like to thank G. Crittenden for reading the manuscript.

REFERENCES

1 Stanway G. Rhinoviruses. *In*: Webster RG, Granoff A, eds. Encyclopedia of Virology. Vol 3. London, Academic Press, 1994; pp. 1253–1259.
2 Nicholson KG, Kent J, Ireland DC. Respiratory viruses and exacerbations of asthma in adults. *BMJ* 1993; 307: 982–986.
3 Seemungal T, Harper-Owen R, Brownmik A, *et al.* Respiratory viruses, symptoms, and inflammatory markers in acute exacerbations and stable chronic obstructive pulmonary disease. *Am J Respir Crit Care Med* 2001; 164: 1618–1623.
4 Sethi S. New developments in the pathogenesis of acute exacerbations of chronic obstructive pulmonary disease. *Curr Opin Infect Dis* 2004; 17: 113–119.
5 Zhu Z, Tang W, Ray A, *et al.* Rhinovirus stimulation of interleukin-6 *in vivo* and *in vitro*. Evidence for nuclear factor κB-dependent transcriptional activation. *J Clin Invest* 1996; 97: 421–430.
6 Subauste MC, Jacoby DB, Richards SM, Proud D. Infection of a human respiratory epithelial cell line with rhinovirus. Induction of cytokine release and modulation of susceptibility to infection by cytokine exposure. *J Clin Invest* 1995; 96: 549–557.
7 Suzuki T, Yamaya M, Sekizawa K, *et al.* Erythromycin inhibits rhinovirus infection in cultured human tracheal epithelial cells. *Am J Respir Crit Care Med* 2002; 165: 1113–1118.
8 Akira S, Hirano T, Taga T, Kishimoto T. Biology of multifunctional cytokines: IL 6 and related molecules (IL 1 and TNF). *FASEB J* 1990; 4: 2860–2867.
9 Allegra L, Cordaro CI, Grassi C. Prevention of acute exacerbations of chronic obstructive bronchitis with carbocysteine lysine salt monohydrate: a multicenter, double-blind, placebo-controlled trial. *Respiration* 1996; 63: 174–180.
10 Carpagnano GE, Resta O, Foschino-Barbaro MP, *et al.* Exhaled interleukin-6 and 8-isoprostane in chronic obstructive pulmonary disease: effect of carbocysteine lysine salt monohydrate (SCMC-Lys). *Eur J Pharmacol* 2004; 505: 169–175.
11 Asti C, Melillo G, Caselli GF, *et al.* Effectiveness of carbocysteine lysine salt monohydrate on models of airway inflammation and hyperresponsiveness. *Pharmacol Res* 1995; 31: 387–392.
12 Sueyoshi S, Miyata Y, Masumoto Y, *et al.* Reduced airway inflammation and remodeling in parallel with mucin 5AC protein expression decreased by *S*-carboxymethylcysteine, a mucoregulant, in the airways of rats exposed to sulfur dioxide. *Int Arch Allergy Immunol* 2004; 134: 273–280.
13 Ishii Y, Kimura T, Morishima Y, *et al.* *S*-carboxymethylcysteine inhibits neutrophil activation mediated by *N*-formyl-methyl-leucyl-phenylalanine. *Eur J Pharmacol* 2002; 449: 183–189.
14 Greve JM, Davis G, Meyer AM, *et al.* The major human rhinovirus receptor is ICAM-1. *Cell* 1989; 56: 839–847.
15 Casasnovas JM, Springer TA. Pathway of rhinovirus disruption by soluble intercellular adhesion molecule 1 (ICAM-1): an intermediate in which ICAM-1 is bound and RNA is released. *J Virol* 1994; 68: 5882–5889.
16 Pérez L, Carrasco L. Entry of poliovirus into cells does not require a low-pH step. *J Virol* 1993; 67: 4543–4548.
17 Suzuki T, Yamaya M, Sekizawa K, *et al.* Bafilomycin A_1 inhibits rhinovirus infection in human airway epithelium: effects on endosome and ICAM-1. *Am J Physiol* 2001; 280: L1115–L1127.
18 Suzuki T, Yamaya M, Sekizawa K, *et al.* Effects of dexamethasone on rhinovirus infection in cultured human tracheal epithelial cells. *Am J Physiol* 2000; 278: L560–L571.
19 Blesa S, Cortijo J, Mata M, *et al.* Oral *N*-acetylcysteine attenuates the rat pulmonary inflammatory response to antigen. *Eur Respir J* 2003; 21: 394–400.
20 Martell M, Gomez J, Esteban JI, *et al.* High-throughput real-time reverse transcription-PCR quantitation of hepatitis C virus RNA. *J Clin Microbiol* 1999; 37: 327–332.
21 Holland PM, Abramson RD, Watson R, Gelfand DH. Detection of specific polymerase chain reaction product by utilizing the 5′–3′ exonuclease activity of *Thermus aquaticus* DNA polymerase. *Proc Natl Acad Sci USA* 1991; 88: 7276–7280.
22 Heid CA, Stevens J, Livak KJ, Williams PM. Real time quantitative PCR. *Genome Res* 1996; 6: 986–994.
23 Amador E, Dorfman LE, Wacker EC. Serum lactic dehydrogenase activity: an analytical assessment of current assays. *Clin Chem* 1963; 9: 391–399.
24 Hofer F, Gruenberger M, Kowalski H, *et al.* Members of the low density lipoprotein receptor family mediate cell entry of a minor group common cold virus. *Proc Natl Acad Sci USA* 1994; 91: 1839–1842.
25 De Schutter JA, Van der Weken G, Van den Bossche W, de Moerloose P. Determination of *S*-carboxymethylcysteine in serum by reversed-phase ion-pair liquid chromatography with column switching following pre-column derivatization with *o*-phthalaldehyde. *J Chromatogr A* 1988; 428: 301–310.
26 Prchla E, Kuechler E, Blaas D, Fuchs R. Uncoating of human rhinovirus serotype 2 from late endosomes. *J Virol* 1994; 68: 3713–3723.
27 Riise GC, Larsson S, Lofdahl CG, Andersson BA. Circulating cell adhesion molecules in bronchial lavage and serum in COPD patients with chronic bronchitis. *Eur Respir J* 1994; 7: 1673–1677.

28 Marshansky V, Vinay P. Proton gradient formation in early endosomes from proximal tubules. *Biochem Biophys Acta* 1996; 1284: 171–180.

29 Brandolini L, Allegretti M, Berdini V, *et al.* Carbocysteine lysine salt monohydrate (SCMC-LYS) is a selective scavenger of reactive oxygen intermediates (ROIs). *Eur Cytokine Network* 2003; 14: 20–26.

30 Bidani A, Reisner BS, Haque AK, *et al.* Bactericidal activity of alveolar macrophages is suppressed by V-ATPase inhibition. *Lung* 2000; 178: 91–104.

MAJOR ARTICLE

Comprehensive Analysis of Bacterial Risk Factors for the Development of Guillain-Barré Syndrome after *Campylobacter jejuni* Enteritis

Michiaki Koga,[1] Michel Gilbert,[4] Masaki Takahashi,[3] Jianjun Li,[4] Saiko Koike,[2] Koichi Hirata,[1] and Nobuhiro Yuki[1]

[1]Department of Neurology and [2]Institute for Medical Science, Dokkyo University School of Medicine, Tochigi, and [3]Department of Microbiology, Tokyo Metropolitan Institute of Public Health, Tokyo, Japan; [4]Institute for Biological Sciences, National Research Council Canada, Ottawa, Ontario, Canada

Background. Guillain-Barré syndrome (GBS), a postinfectious autoimmune-mediated neuropathy, is a serious complication after *Campylobacter jejuni* enteritis.

Methods. To investigate the bacterial risk factors for developing GBS, genotypes, serotypes, and ganglioside mimics on lipo-oligosaccharide (LOS) were analyzed in *C. jejuni* strains from Japanese patients.

Results. Strains from patients with GBS had LOS biosynthesis locus class A more frequently (72/106; 68%) than did strains from patients with enteritis (17/103; 17%). Class A strains predominantly were serotype HS:19 and had the *cstII* (Thr51) genotype; the latter is responsible for biosynthesis of GM1-like and GD1a-like LOSs. Both anti-GM1 and anti-GD1a monoclonal antibodies regularly bound to class A LOSs, whereas no or either antibody bound to other LOS locus classes. Mass-spectrometric analysis showed that a class A strain carried GD1a-like LOS as well as GM1-like LOS. Logistic regression analysis showed that serotype HS:19 and the class A locus were predictive of the development of GBS.

Conclusions. The high frequency of the class A locus in GBS-associated strains, which was recently reported in Europe, provides the first GBS-related *C. jejuni* characteristic that is common to strains from Asia and Europe. The class A locus and serotype HS:19 seem to be linked to *cstII* polymorphism, resulting in promotion of both GM1-like and GD1a-like structure synthesis on LOS and, consequently, an increase in the risk of producing antiganglioside autoantibodies and developing GBS.

The gram-negative spiral bacterium *Campylobacter jejuni*, which is a major bacterial agent in diarrheal illnesses, has been recognized as the bacterium that most frequently triggers the postinfectious autoimmune-mediated neuropathy called Guillain-Barré syndrome (GBS) [1]. An epidemiological study showed that 1 of 3285 patients with *C. jejuni* enteritis developed GBS [2]. Why such a small number of patients with *C. jejuni* enteritis develop GBS is not clear. Penner serotyping showed that, in Japan and South Africa, GBS-associated strains were more commonly serotypes HS:19 and HS:41 than were enteritis-associated strains [3–5]. Furthermore, HS:2 and the HS:4-complex were the dominant serotypes of strains from patients with Fisher syndrome (FS) [5], a GBS variant presenting the triad of ophthalmoplegia, ataxia, and areflexia [6]. The clustering of strains into particular serotypes is a strong indication that the clonality of *C. jejuni* strains is specifically related to the development of GBS and FS. The actual serodeterminants, however, are still unknown [7]; therefore, use of Penner serotyping schema alone to clarify the critical factors for the development of neurological syndromes would be difficult. It is noteworthy that the clustering of GBS-associated and FS-associated strains into specific serotypes has not been

Received 21 June 2005; accepted 20 September 2005; electronically published 19 January 2006.

Potential conflicts of interest: none reported.

Financial support: Ichiro Kanehara Foundation (grant to M.K.); Kanae Foundation for Life and Socio-Medical Science (grant to M.K.); Japan Intractable Diseases Research Foundation (grant to M.K.); Dokkyo University School of Medicine (grant 2005-01-2 to M.K.); Mizutani Foundation for Glycoscience (grant to N.Y.); Ministry of Education, Culture, Sports, Science, and Technology of Japan (scientific research [B] grant Kakenhi 16390254 to N.Y.); Ministry of Health, Labor, and Welfare of Japan (health sciences research grant for psychiatric and neurological diseases and mental health and health and labor sciences research grant on measures for intractable diseases 17243601 to N.Y.); Human Frontier Science Program (grant RGP0038/2003-C to M.G. and N.Y.).

Reprints or correspondence: Dr. Michiaki Koga, Dept. of Neurology, Dokkyo University School of Medicine, Kitakobayashi 880, Mibu, Shimotsuga, Tochigi 321-0293, Japan (kogamrk@dokkyomed.ac.jp).

The Journal of Infectious Diseases 2006; 193:547–55

© 2006 by the Infectious Diseases Society of America. All rights reserved.

0022-1899/2006/19304-0010$15.00

seen worldwide and, in particular, has not been seen in Western countries [8, 9].

Most patients who develop GBS after *C. jejuni* enteritis have IgG autoantibodies in their blood that react with gangliosides (such as GM1, GD1a, and GQ1b) [10]. Many patients with FS have anti–GQ1b IgG autoantibodies that cross-react with GT1a [11, 12]. The *C. jejuni* lipo-oligosaccharide (LOS) is a major candidate for the producer of such autoantibodies [13–15], because its terminal sugar regions mimic the gangliosides GM1, GD1a, and GQ1b [16–18]. The frequency of the GM1 and GD1a epitopes on the LOS of GBS-associated strains is hypothesized to be a risk factor for the development of GBS [19, 20]. Acute motor axonal neuropathy and anti-GM1 antibodies developed in rabbits after inoculation with GM1-like LOS, which indicates that GM1 mimicry of *C. jejuni* LOS is a cause of GBS [14].

Most studies have failed to find a specific *C. jejuni* genotype that was associated with GBS and FS [9, 21–24]. Gilbert et al. [25] reported that *C. jejuni* has 7 classes (A–G) of LOS locus that are based on the organization of the 37 distinct genes found in the LOS biosynthesis loci of 20 strains. This LOS locus typing scheme should help in the identification of the gene content that is responsible for the development of GBS and FS. Godschalk et al. [15], who used clinical isolates from The Netherlands and Belgium, recently reported that the class A locus was overrepresented in GBS-associated strains, compared with enteritis-associated strains (9/17 [53%] vs. 3/21 [14%]), whereas all FS-associated strains had the class B locus (FS-associated strains, 4/4 [100%]; enteritis-associated strains, 7/21 [33%]). The high frequency of the class A locus in GBS-associated strains has been confirmed by Parker et al. [26], who used 16 GBS-associated strains from various countries, although the frequency of this locus in GBS-associated strains could not be compared with that in enteritis-associated strains from each country. Godschalk et al. [15] suspected that the frequent expression of a GM1-like LOS in class A strains and a GQ1b-like LOS in class B strains is responsible for the development of GBS and FS, respectively. Their findings, however, do not clarify which genetic difference leads to the presence of diverse ganglioside mimics (GM1 and GQ1b) in spite of the almost identical gene profiles in class A and B loci [27] or why class C is relatively rare (2/17 [12%]) in GBS-associated strains in spite of the expression of GM1-like LOSs in all 5 strains with the class C locus.

The sialyltransferase gene *cstII* has an Asn/Thr polymorphism at codon 51, which determines substrate specificity; *cstII* (Thr51) has only α-2,3-sialyltransferase activity and is termed "monofunctional" *cstII*, whereas *cstII* (Asn51) has both α-2,3- and α-2,8-sialyltransferase activities and is termed "bifunctional" *cstII* [27]. Both sialyltransferase activities are required for the biosynthesis of the GQ1b and GT1a epitopes on LOS, whereas only α-2,3-sialyltransferase activity is needed for the biosynthesis of the GM1 and GD1a epitopes (figure 1). These findings recently led to our discovery that *cstII* polymorphism is important for the development of GBS and FS after *C. jejuni* enteritis [29]. *cstII* (Thr51) is closely associated with GBS and anti-GM1 and anti-GD1a autoantibodies, and *cstII* (Asn51) is closely associated with FS and anti-GQ1b autoantibodies.

Some of the identified bacterial risk factors for the development of GBS are closely related to each other, especially ganglioside mimics and serotype [19], *cstII* gene content [19, 29], and LOS locus class [15]. Therefore, it is necessary to analyze the risk factors comprehensively in a larger number of clinical isolates. We first examined whether the clustering of GBS-associated and FS-associated strains into a specific LOS locus class would also occur with a large number of Japanese strains; we then analyzed LOS locus classes comprehensively in connection with Penner serotype, *cstII* polymorphism, and ganglioside-like LOSs, to identify risk factors for the development of GBS.

MATERIALS AND METHODS

Strains. From December 1990 to February 2004, 138 *C. jejuni* strains were isolated from patients with GBS (n = 106) or FS (n = 32), and these strains were used in the present study. Most of the strains were included in our previous study [5]. Two strains, OH4384 and OH4382, were obtained from patients with GBS who were siblings [17, 30], and the others were obtained from patients with GBS who were evenly distributed geographically [5]. Diagnosis of GBS or FS was based on published clinical criteria [31, 32]. A total of 103 strains were isolated from patients throughout Japan who had uncomplicated enteritis, and these strains served as controls. Penner serotypes were determined using the passive hemagglutination technique with a *Campylobacter* antisera "Seiken" Set (Denka Seiken) [5].

LOS locus classification and* cstII *polymorphism. We used a method similar to that of Godschalk et al. [15] to classify the LOS locus (A–F). The presence of each class-specific gene was investigated by polymerase chain reaction (PCR) (table 1). The primer pair used for *orf19d* amplification was the same as that used in the study by Godschalk et al. [15], whereas the other primer pairs were newly designed for the present study. Class G was not examined, because it is considered to be very rare. Strains were judged to be class A when *orf7a/b (cstII)* was present and *orf5IIb (cgtAIIb)* was absent. Similarly, strains were judged to be class F when *orf19d/f* was present and *orf17d* was absent. A single bacterial colony was suspended in 300 μL of sterile distilled water and boiled for 10 min. After centrifugation at 10,000 *g* for 1 min, the supernatant was used as the template in the PCR amplification. Amplification reactions were performed with a total volume of 20 μL, which contained 8 pmol of each primer, 0.4 μL of DNA lysate, 0.5 U of *Taq* DNA

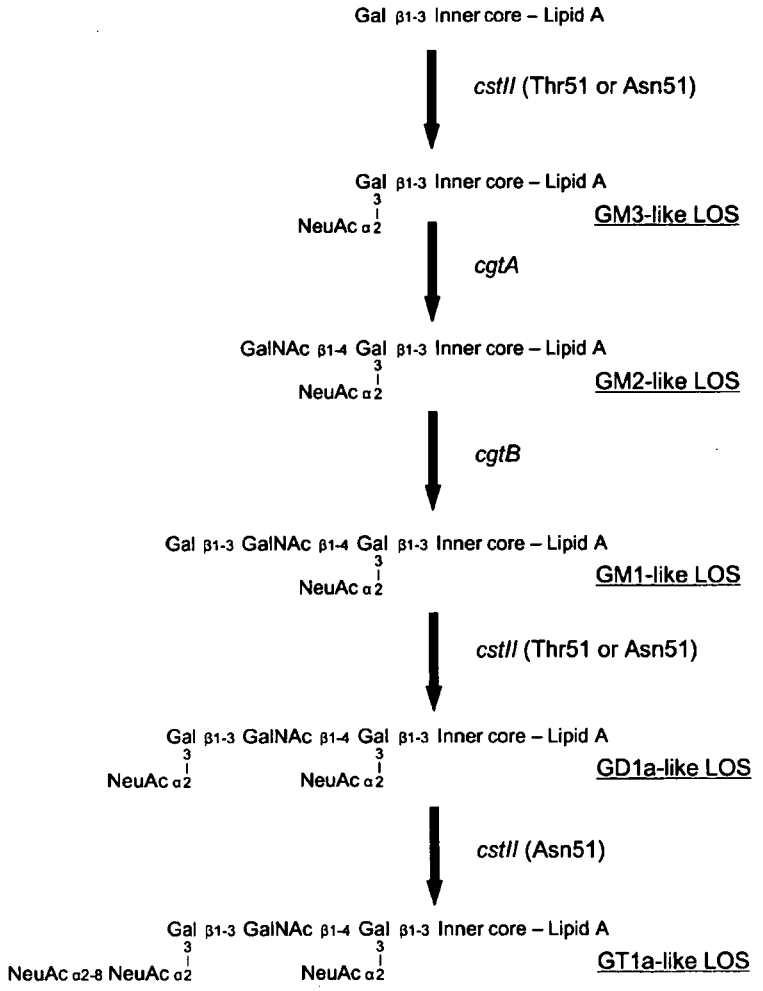

Figure 1. Proposed biosynthesis pathway of *Campylobacter jejuni* lipo-oligosaccharides (LOSs) mimicking gangliosides with a single sialic acid on the inner galactosyl residue [27, 28]. Gal, galactose; GalNAc, *N*-acetylgalactosamine; NeuAc, *N*-acetylneuraminic acid.

polymerase (TaKaRa Ex Taq; Takara Bio), 4 nmol of dNTPs, and buffer (2 mmol/L Mg^{2+}). After the first denaturation step of 5 min at 95°C, the amplification mixture was subjected to 30 cycles of amplification (table 1). Variation at codon 51 of *cstII* was investigated by direct sequencing of the PCR fragment [29].

Ganglioside-like LOS. Crude LOS fractions were prepared from the strains as described elsewhere [33]. The presence of ganglioside epitopes (GM1, GD1a, and GQ1b) on the *C. jejuni* LOS was determined using an ELISA [34]. The reagents used were monoclonal antibodies (mAbs; GB2 [anti-GM1], GB1 [anti-GD1a], and FS3 [anti-GQ1b/GT1a]) [14, 34].

Analysis of O-deacylated LOS. *C. jejuni* was grown overnight on a single agar plate, and the cells were treated as described elsewhere [35], with minor modification [34]. The *O*-deacylated LOS sample was analyzed by capillary electrophoresis–electrospray ionization mass spectrometry (CE-ESI-MS) [36].

Sequencing of LOS biosynthesis genes. Isolation of genomic DNA from *C. jejuni* strain CF90-26 was performed with a DNeasy Tissue kit (Qiagen). A 6.1-kb PCR product bearing genes encoding the LOS outer core glycosyltransferases was amplified with an Advantage 2 PCR kit (Clontech Laboratories) and the primers CJ-99 (5′-ATTAAAAAAAGACCTTGGGAATAC-3′) and CJ-147 (5′-AAGGTGTGCTAAGATAAACAAGAC-3′). The 6.1-kb PCR

Table 1. Polymerase chain reactions for the lipo-oligosaccharide gene loci of *Campylobacter jejuni* strains.

The table is available in its entirety in the online edition of the *Journal of Infectious Diseases*.

Table 2. Lipo-oligosaccharide (LOS) locus classes of *Campylobacter jejuni* strains.

LOS locus class	Guillain-Barré syndrome–associated strains (n = 106)		Fisher syndrome–associated strains (n = 32)		Enteritis-associated strains, no. (%) (n = 103)
	No. (%)	2-tailed P[a]	No. (%)	2-tailed P[a]	
A	72 (68)	<.001	12 (38)	.02	17 (17)
B	18 (17)	.02	15 (47)	.14	33 (32)
C	12 (11)	.13	1 (3)	.03	20 (19)
D	0	.12	0	1.0	3 (3)
E	2 (2)	.001	2 (6)	.36	14 (14)
F	0	.01	0	.34	6 (6)
A/C[b]	0	.49	0	1.0	1 (1)
B/C[c]	0	.49	0	1.0	1 (1)
Unclassified	2 (2)	.06	2 (6)	1.0	8 (8)
A, B, or C	102 (96)	<.001	28 (88)	.06	72 (70)

[a] Compared with enteritis-associated strains (Fisher's exact test).
[b] Overlapping class A and C loci.
[c] Overlapping class B and C loci.

product was sequenced by means of custom-made primers that were used previously to sequence this locus in multiple *C. jejuni* strains [27]. DNA sequencing was performed with a BigDye Terminator mix (Applied Biosystems). Products were analyzed in an ABI 3100 Genetic Analyzer (Applied Biosystems).

Antiganglioside autoantibodies. Serum samples obtained during acute phases of GBS and FS were available from 126 patients (95 patients with GBS and 31 patients with FS). IgG autoantibodies to GM1, GD1a, and GQ1b were measured by ELISA [37]. Serum was considered to be positive for antibody when the titer was ≥500.

Statistical analysis. Frequency differences between groups were compared using Fisher's exact test. Differences in medians were examined using the Mann-Whitney U test, and Scheffé's test was used in the case of multiple comparisons. The association between the LOS locus class and either GBS or FS was first investigated by univariate analysis, without adjustment for confounding variables. A multiple logistic regression model was then used to determine the relative weighting of each variable. Statistical calculations were made with SPSS (version 12.0J; SPSS). A difference was considered to be statistically significant when $P < .05$.

RESULTS

LOS locus classification. Preliminary analysis of control strains of each LOS locus class confirmed that PCR-based LOS locus classification works well (data not shown). The class A locus was predominant in the GBS-associated strains, and its frequency was significantly higher in GBS-associated strains than in enteritis-associated strains (table 2). The other LOS locus classes were rarer in GBS-associated strains than in enteritis-associated strains. These findings agree with those of Godschalk et al. [15]. In contrast, FS-associated strains most frequently had the class B locus, but, compared with the enteritis-associated strains, the difference did not reach statistical significance, because it also was the most common class found in enteritis-associated strains. In the study by Godschalk et al. [15], all 4 FS-associated strains had the class B locus, whereas, in the present study, a significant number of FS-associated strains had the class A locus. In 12 strains (2 GBS associated, 2 FS associated, and 8 enteritis associated), there was no amplification of any class-specific genes. Two enteritis-associated strains were grouped as having overlapping class A and C or B and C loci.

Sialyltransferase-encoding genes (*cstII* or *cstIII*) are present in class A, B, and C loci [27], and this enables strains with these LOS locus classes to be characterized as a single group. Our data showed that 96% of GBS-associated strains had sialyltransferase-carrying LOS locus classes (A, B, or C), and this percentage was significantly higher than that of enteritis-associated strains (70%) (table 2). FS-associated strains also regularly had these LOS locus classes (88%).

Serotype. Table 3 shows the associations between the LOS locus class and the Penner serotype in GBS-associated, FS-associated, and enteritis-associated strains. LOS locus classes were closely—but not absolutely—associated with the Penner serotype, because strains with each LOS locus class were grouped into several serotypes, as was reported by Parker et al. [26]. Most class A strains were serotype HS:19, whereas the serotypes of class B strains varied. Conversely, most of the HS:19 strains had the class A locus, whereas most of the HS:2 and HS:4-complex strains had the class B or A locus.

cstII *polymorphism.* Class A and B loci are reported to carry the *cstII* gene [27]. Therefore, the association between *cstII* polymorphism and the class A or B locus was examined. Most of the class A strains had the *cstII* (Thr51) genotype (78/

Table 3. Associations between lipo-oligosaccharide (LOS) locus class and Penner serogroup in *Campylobacter jejuni* strains.

LOS locus class	Strains, no.	Serogroup (serotype) A (HS:1/44)	B (HS:2)	D (HS:4/13/16/43/50)	G (HS:8)	O (HS:19)	Y (HS:37)	Other
A[a]	101	0	7 (7)	15 (15)	0	73 (72)	1 (1)	6 (6)
B	66	1 (2)	21 (32)	21 (32)	6 (9)	6 (9)	0	17 (26)
C[b]	33	14 (42)	7 (21)	0	5 (15)	0	0	8 (24)
D	3	0	0	0	0	0	0	3 (100)
E	18	0	0	0	0	0	8 (44)	10 (56)
F	6	0	1 (17)	0	0	0	0	5 (83)
A/C	1	0	1 (100)	0	0	0	0	0
B/C	1	0	0	0	0	0	0	1 (100)
Unclassified	12	2 (17)	2 (17)	0	0	2 (17)	0	6 (50)

NOTE. Data are no. (%) of strains, unless otherwise indicated.

[a] One strain was serotyped as the O/Y serogroup.

[b] One strain was serotyped as the A/G serogroup.

101; 77%), whereas most of the class B strains had the *cstII* (Asn51) genotype (49/66; 74%). FS-associated strains, however, were closely associated with the *cstII* (Asn51) genotype, irrespective of whether the LOS locus class was A or B; 8 (80%) of 10 class A strains and all 12 (100%) class B strains had the *cstII* (Asn51) genotype. This suggests that *cstII* polymorphism, and not LOS locus class, is critical for the development of FS.

Ganglioside-like LOS and antiganglioside autoantibodies. On the whole, reactivity to anti-GM1 mAb was increased in class A and C strains, and that of anti-GD1a mAb was increased only in class A strains (figure 2); this is indicative of a difference in sialyltransferase substrate specificity between classes A *(cstII)* and C *(cstIII)* [25]. Some class B strains had high reactivity to anti-GM1 and anti-GD1a mAbs, but the median optical density was low. Reactivity to anti-GQ1b/GT1a mAb was high overall in class B strains and in some class A strains, but it was not high in strains with loci of other classes.

We defined ganglioside epitopes as being present on LOSs when the OD of mAb in the ELISA was $\geq$0.2. There was an obvious difference in ganglioside epitopes between strains with the class A, B, or C locus and strains with the class D, E, or F locus, with epitopes being frequent in the former group and absent in the latter group. For example, the GM1 epitope was judged to be present in 80% of class A strains, 26% of class B strains, and 64% of class C strains but in none of the strains with the class D, E, or F locus. Furthermore, class A strains regularly expressed both the GM1 and has the GD1a epitope, whereas class C strains expressed only the GM1 epitope; the GD1a epitope was detected in 76% of class A strains but in only 3% of class C strains. The GQ1b/GT1a epitope was present in 37% and 50% of class A or B strains, respectively; no strain with the class C, D, E, or F locus had this epitope. Notably, several unclassified strains also had ganglioside-mimicking LOS (figure 2), and this is indicative of an unknown sialyltransferase gene being present at an unclassified locus.

Patients with class A or C strains often were positive for IgG autoantibodies against GM1 (72% and 75%, respectively). Interestingly, the frequency of anti-GD1a IgG autoantibodies was higher in patients with class A strains (51%) than in patients with class C strains (33%). These data agree with the finding that anti-GD1a mAb bound to class A LOS but not to class C LOS. In contrast, patients with class B strains more commonly had anti-GQ1b IgG autoantibodies (44%) than anti-GM1 IgG autoantibodies (25%) or anti-GD1a IgG autoantibodies (25%). Anti-GQ1b IgG autoantibodies were rarely detected in patients with class A (14%) or class C (0%) strains. These data agree with the finding that anti-GQ1b/GT1a mAb regularly bound to class B LOS.

LOS structure and glycosyltransferase genes of strain CF90-26. Because the above data suggested the importance of the GM1 and GD1a epitopes on class A strains, we investigated in detail the LOS structure and gene sequences of the *cstII, cgtA,* and *cgtB* glycosyltransferase genes. Elsewhere, we showed that *C. jejuni* strain CF90-26 (a serotype HS:19 class A strain from a patient with GBS who had high anti–GM1 IgG autoantibody titers), which was used in the present study, has a GM1-like structure, on the basis of nuclear magnetic resonance analysis [16], and has the GD1a epitope, on the basis of thin-layer chromatography with immunostaining [38]. CE-ESI-MS analysis of an *O*-deacylated LOS sample from *C. jejuni* strain CF90-26 yielded various masses, and the predominant species was $[M-4H]^{4-}$ (3645 Da). The differences in observed masses (table 4) were due to lipid A variation, as well as to the presence or absence of a terminal sialic acid (in addition to the sialic acid that is present on the inner galactosyl residue). CE-ESI-MS analysis showed that the absence of the terminal sialic acid resulted in a GM1 mimic, and its presence in a GD1a mimic (figure 3) provided evidence that CF90-26 has both GM1-like and GD1a-like LOSs. The LOS biosynthesis gene sequence in strain CF90-26 (GenBank accession number AY661458) was